Influence of a finite scattering volume on the determination of electron-impact coherence parameters

P. W. Zetner* and S. Trajmar

Jet Propulsion Laboratory, California Institute of Technology, Pasadena, California 91109

G. Csanak

Los Alamos National Laboratory, Los Alamos, New Mexico 87545

(Received 13 November 1989)

Superelastic electron scattering from laser-excited ^{138}Ba(. . .$6s\,6p\ ^1P$) is investigated both theoretically and experimentally. The theoretical framework is developed and incorporated into a model of a realistic scattering geometry of finite spatial extent. Model calculations predict that the dependence of the superelastic scattering intensity on the linear polarization direction of the laser beam can be severely distorted due to the existence of a finite scattering volume. Our measurements confirm the presence of this distortion and are well described by the model calculations. Conclusions are drawn concerning the influence of this effect on the extraction of electron-impact coherence parameters.

I. INTRODUCTION

In an ideal electron–atom-beam scattering experiment, the interaction region defined by the intersecting beams and the view cone of the detector should be small in comparison with other characteristic dimensions of the scattering geometry, and the energy and angular resolution of the apparatus should be narrow with respect to the ranges over which quantities of interest undergo significant changes. In this case, the scattering signal can be assumed to originate from a pointlike scattering center, and the data obtained from the measurements can be assigned to well-defined electron-impact energy (E_0) and scattering angle (θ_e). In practice, the dimensions of the scattering volume and the energy and angular resolution of the apparatus are always finite, and a rigorous treatment of the scattering data should take this into account. In conventional electron scattering measurements of the differential scattering cross section (DCS) or related quantities these considerations, in general, cause no serious problem. The measured DCS can then be associated with nominal scattering angles (defined by the geometry of the instrument) and impact energies, but represents an average over the unresolved range of these parameters. A discussion of these matters in electron scattering DCS measurements has been given, for example, by Brinkmann and Trajmar.[1]

The 1970s heralded the application of coincidence techniques to electron-atom or -molecule collision experiments. In particular, electron-photon coincidence experiments have made accessible to measurement the orientation and alignment parameters of the target state created by the collision process.[2,3] A more fundamental aspect of the collision physics thus became open to investigation. Closely related to electron-photon coincidence experiments are the superelastic electron scattering experiments on laser-excited targets introduced by Hertel and

Stoll.[4] A large body of data has been accumulated in these very active fields both from experimental and theoretical efforts as summarized in the recent review of Andersen, Gallagher, and Hertel.[5] It is also clear from this review that, in some cases, substantial disagreement exists between experiment and theory and even among measurements carried out by various investigators.

So far, in measurements of electron-impact coherence parameters (EICP), it has been conventionally assumed that the data obtained in the experiment can be interpreted as scattering by a pointlike target located at the origin of some laboratory or reference frame. Martus, Becker, and Madison[6] discussed the effect of finite resolution in scattering angle on the measurement of EICP and showed how the convolution by the detector angular resolution distorts these parameters. However, the fact that the scattering signal arises from an ensemble of scattering points, distributed within a finite effective scattering volume, can have more serious effects on the measurements of EICP than those accounted for by averaging over scattering angles alone. Scattering signal arising from the finite scattering volume cannot be associated with a precisely defined scattering plane but instead represents the contribution from a set of different scattering planes defined by different collision events occurring within the extended volume. Hence an average over scattering planes occurs which can significantly influence an EICP measurement. It is easy to visualize and anticipate these problems at near-zero scattering angles, but a detailed analysis shows that these geometrical effects may be amplified by the behavior of the EICP themselves and persist over a wide range of scattering angles.

The present paper focuses upon the superelastic scattering of electrons from ^{138}Ba($6s6p\ ^1P_1$) atoms which have been excited by linearly polarized laser radiation with the direction of incidence lying in the plane defined by the electron gun and detector. Such an experiment has been reported by Register *et al.*[7] In their work, it

was assumed, as in common practice, that the scattering process could be described in terms of a pointlike scattering center. These investigators found an asymmetry in the superelastic scattering signal I^S as a function of laser polarization angle ψ. Contrary to theoretical predictions for the system they studied, they found that $I^S(\psi) \neq I^S(-\psi)$. This asymmetry was expressed as a modulation phase shift whose behavior could not be altered despite exhaustive tests under wide ranging variations in the experimental conditions. Recently, we have reinvestigated this question and have found basically the same behavior as that observed by Register et al.[7] However, during these studies, we discovered some clues which led to the understanding of this asymmetry as well as to the realization that the measurements of EICP may be seriously influenced by the unavoidable reality of a scattering target volume of finite dimension.

There have been three important developments that have allowed us to recognize and evaluate the influence of a realistic, finite scattering geometry: (a) the ability to calculate EICP for Ba, (b) the development of a modeling code to treat scattering by an extended target and, (c) the recognition that the detector spatial response plays a critical role in defining the effective scattering volume. We undertook a study involving modeling calculations and supporting laboratory experiments to elucidate the importance of efforts caused by a finite scattering geometry. In this paper, we examine in detail the case of superelastic electron scattering from ^{138}Ba($6s6p$ $^1P_1$) atoms excited by a linearly polarized laser beam as described by Register et al.[7] The EICP were obtained from the calculations of Clark et al.[8] The analysis reveals that the asymmetry observed by Register et al.[7] can be explained by geometrical effects and the reason for their inability to tie this asymmetry to the scattering geometry is now understood. Furthermore, we found that the finite geometry seriously influences the modulation depth of the superelastic scattering signal $I^S(\psi)$ and thus leads to large errors in the determination of the EICP under the assumption of a single point scatterer which in turn can lead, for example, to erroneous conclusions about the magnitude of spin-orbit coupling effects in the scattering. A brief summary of these results has been published earlier.[9]

This work is organized as follows. Section II gives the theoretical formalism for $J=1$ to $J_0=0$ superelastic scattering. This section is essentially a recapitulation of the work of Macek and Hertel[10] and the implementation of their general formulas for our case. Section III discusses the incorporation of this theory into a model of a realistic experimental geometry. The role played by the extended scattering volume and the finite angular resolution of the electron detector as well as the averaging process associated with other experimental parameters is examined. Section IV outlines a series of experiments performed to alter the relevant aspects of the scattering geometry in a controlled fashion and provide a check on the model calculations. Comparison of the experimental results with modeling results are also made in this section. A brief discussion and summary of the pertinent points are given in Sec. V.

II. THEORY

A. General remarks

The theoretical foundation for the analysis of electron scattering by laser-excited targets was developed by Macek and Hertel[10] in a compact form based on the formalism of state multipoles of Fano.[11] The essential result of their analysis is that the superelastic scattering experiment provides information about the state of the target which would be prepared in a hypothetical time-inverse (inelastic) scattering experiment and which would be observed in an electron-photon coincidence experiment. If spin-orbit coupling enters the scattering process, a superelastic scattering will not be exactly the inverse of an inelastic process. The information obtained from the two experiments, however, will be identical if the incident electron beams are not spin polarized and the spin of the scattered electrons is not detected. We will refer to this hypothetical inelastic scattering process as the *inelastic collision process*. The target state prepared by the scattered electron in the inelastic collision process is, in general, a mixed state and as such it can be characterized by a density matrix[12] or equivalently by the state multipoles of Fano,[11] by the orientation and alignment parameters of Fano and Macek,[13] or, in the case of $J_0=0\rightarrow J=1$ transition, by the EICP of da Paixão et al.,[14] by other equivalent parameters.[5] The only modification of the Macek-Hertel theory will be the relaxation of the Percival and Seaton[15] adiabatic hypothesis. This hypothesis assumes that the electronic angular momentum and nuclear spin or the electronic orbital angular momentum and electronic spin are uncoupled during the collision process, and the collision does not affect the nuclear-spin state or the electronic-spin state, respectively. For Ba, in the intermediate coupling scheme, the $6s6p$ $^1P_1$ level is described as a linear combination of LS-coupled $^1P_1$ and $^3P_1$ states. In the present formalism, we relax the Percival-Seaton hypothesis and assume that, in the superelastic scattering process, the incident electron impulsively deexcites a $|JM_J\rangle$ state. (As we shall see, the theoretical calculations show that the Ba $^1P_1$ state is essentially LS coupled and thus this assumption is rather academic.) Since the experiment deals with the ^{138}Ba, the nuclear spin, $I=0$ and the adiabatic hypothesis need not be discussed for the nuclear spin.

B. Fundamental concepts and formulas

The laser-pumping process prepares an ensemble of atoms characterized by a state which is, in general, a partially coherent mixture of the various magnetic sublevels of the excited level. This ensemble can be described, in general, by a density matrix or by the equivalent density operator. It has been shown by Macek and Hertel[10] that, for pumping by linearly or circularly polarized light, one can define a coordinate system, called the *photon frame*, in such a way that the density matrix will be diagonal in that coordinate system. Let us denote by F and M_F the total angular momentum quantum numbers associated with the excited atom and its projection to the Z axis of

the photon frame (Z_{ph}), respectively. Denote by $|nFM_F\rangle$ the state vector of a sublevel belonging to the level n,F.[16] Here n refers to the additional quantum numbers necessary to identify the excited atomic level. Macek and Hertel have shown that, under these conditions, the *density operator* $\hat{\tau}$ of the excited state generated by the laser pumping process will have the form

$$\hat{\tau}= \sum_{M_F} W(M_F)|nFM_F\rangle\langle nFM_F| ,\tag{1}$$

where $W(M_F)$ is the probability that the $|nFM_F\rangle$ state was prepared by the laser-pumping process. For the ^{138}Ba isotope, the nuclear spin, $I=0$ and consequently, $F=J$ and $M_F=M_J$, where J and M_J refer to the quantum numbers of the total electronic angular momentum and its projection onto the Z_{ph} axis, respectively. The $|nFM_F\rangle$ state can therefore be written as

$$|nFM_F\rangle=|nJM_J\rangle|00\rangle ,\tag{2}$$

where $|nJM_J\rangle$ describes the electronic state and $|00\rangle$ the state of the nucleus, giving for $\hat{\tau}$

$$\hat{\tau}= \sum_{M_J} W(M_J)|nJM_J\rangle\langle nJM_J||00\rangle\langle 00| .\tag{3}$$

The factor $|00\rangle\langle 00|$ is the unit operator in the nuclear-spin space of the ^{138}Ba atom it can be completely ignored in the formal treatment. Thus we will define $\hat{\tau}$ in the form

$$\hat{\tau}= \sum_{M_J} W(M_J)|nJM_J\rangle\langle nJM_J| .\tag{4}$$

In the following all $|\rangle$ and $\langle|$ will refer to electronic states of the ^{138}Ba atom. If the electronic collision process can be described within the LS-coupling scheme, and $|nJM_J\rangle$ is a pure LS-coupled single state (as is the case here), then the $J=L$ and $M_J=M_L$ identification can be made and one can write $|nLM_L\rangle=|nLM_L\rangle|00\rangle$, where $|nLM_L\rangle$ refers to the orbital part of the wave function. In the following we will not make this assumption to keep the analysis more general. The reason for keeping a non-LS-coupled description is many fold. First, spin-orbit-coupling effects may enter the description of the continuum electron and then it is more consistent to allow for those kind of effects in the target also. Second, it allows us to show that not considering volume-correction effects erroneous conclusions can be obtained with respect to the importance of the spin-orbit coupling effect for the coherence parameters. Third, the LS-coupled nature of the target comes from a theoretical calculation which incorporates some semiempirical parameters describing relativistic effects.[8] A completely *ab initio* calculation may show some spin-orbit-coupling effects in the relevant target states.

With the above definition of $\hat{\tau}$, it has been shown by Macek and Hertel[10] that the superelastic scattering intensity I^S can be given in the form

$$I^S=C \sum_{M_{J_0},m_{s_1},m_{s_2}} \frac{1}{2J_0+1}\frac{1}{2}\langle \psi_n(J_0M_{J_0}m_{s_1}m_{s_2})|\hat{\tau}|\psi_n(J_0M_{J_0}m_{s_1}m_{s_2})\rangle ,\tag{5}$$

where C is a constant consisting of multiplicative factors such as detection solid angle, detection efficiency, the number of atoms in the optically pumped level nJ, the flux of the incident electrons, and the differential superelastic scattering cross section for fixed scattering angle and energy. The state vector of the state that would be prepared by the inelastic electron collision process with well-defined initial and final electron spins appearing in Eq. (5) is defined by

$$|\psi_n(J_0M_{J_0}m_{s_1}m_{s_2})\rangle$$

$$= \sum_{J,M_J} f(nJM_J\mathbf{k}_2m_{s_2},n_0J_0M_{J_0}\mathbf{k}_1m_{s_1})|nJM_J\rangle ,\tag{6}$$

where $f(nJM_J\mathbf{k}_2m_{s_2},n_0J_0M_{J_0}\mathbf{k}_1m_{s_1})$ is the scattering

amplitude for electron-impact excitation of the $|nJM_J\rangle$ excited state of the atomic target from the $|n_0J_0M_{J_0}\rangle$ ground state with m_{s_1} and m_{s_2} referring to the spins, and $\mathbf{k}_1$ and $\mathbf{k}_2$ to the momenta of the incident and inelastically scattered electrons, respectively. In obtaining Eq. (5), it was assumed that the incident electron beam is unpolarized and that the spin polarization of the superelastically scattered electrons is not detected.[17]

Equation (4) was converted into a more transparent from by Macek and Hertel[10] with the introduction of the *density operator* $\hat{\rho}$ of the state that would be prepared in the inelastic collision process involving initially unpolarized electron and atomic beams and polarization insensitive detector. This operator can be defined by the formula

$$\hat{\rho}= \frac{\displaystyle\sum_{M_{J_0},m_{s_1},m_{s_2}} \frac{1}{2J_0+1}\frac{1}{2}|\psi_n(J_0M_{J_0}m_{s_1}m_{s_2})\rangle\langle \psi_n(J_0M_{J_0}m_{s_1}m_{s_2})|}{\displaystyle\sum_{M_{J_0}m_{s_1}m_{s_2}} \frac{1}{2J_0+1}\frac{1}{2}|f(nJM_J\mathbf{k}_2m_{s_2},n_0J_0M_{J_0}\mathbf{k}_1m_{s_1})|^2} .\tag{7}$$

This density operator characterizes a partially coherent state prepared in the inelastic collision process. Using Eq. (7) in Eq. (5) one obtains the fundamental formula of Macek and Hertel[10]

$$I^S = \bar{C} \, \text{tr} \hat{\rho} \, \hat{\tau} \equiv \bar{C} \langle \hat{\tau} \rangle \, , \tag{8}$$

where tr refers to the trace of an operator in the state-vector space of the atomic targets and $\langle \ \rangle$ refers to the average with respect to the state characterized by the density operator $\hat{\rho}$. $\bar{C}$ is equal to C times the denominator of Eq. (7). Equation (8) expresses compactly the fact that the superelastic scattering intensity provides information about $\hat{\rho}$, since $\hat{\tau}$ is defined by the laser pumping process [see Eq. (1)]. It also shows the dependence of I^S upon laser-polarization properties and laser-incidence angle through $\hat{\tau}$, which is dependent upon these parameters.

From now on let us consider the special case of pumping by linearly polarized laser light a $J_0 = 0$ state to a $J = 1$ state (which corresponds to the experiment described here and in Ref. 6). In this case, as was shown in Macek and Hertel,[10] $\hat{\tau}$ can be given as

$$\hat{\tau} = |n10\rangle\langle n10| \, , \tag{9}$$

assuming that the axis of quantization Z_{ph} was selected along the polarization vector $\hat{e}_\nu$ of the incident laser light. It can be seen that, in this special case, the state prepared by the pumping process is a completely coherent state of the Ba atom. This is due to the fact that the ground state of Ba is a nondegenerate $^1S_0$ state and the laser-pumping mechanism is simple compared, for example, to Na.

The superelastic scattering experiment provides information about the inelastic scattering process which is conveniently described in the collision frame associated with this inverse process. In order to obtain explicitly the angular dependences of I^S, the operator $\hat{\tau}$ has to be transformed into the collision frame. First, however, we have to define precisely the various coordinate systems which enter the analysis.

C. Coordinate systems

In the superelastic scattering experiment the electrons are characterized by the momentum of the incident electron $(\mathbf{k}_i)$ and the momentum of the superelastically scattered electron $(\mathbf{k}_f)$. For the inverse inelastic process we use the notation of $\mathbf{k}_{\text{in}}$ and $\mathbf{k}_{\text{out}}$ for the momentum of the incident and scattered electrons, respectively (to be consistent with the notation of Andersen, Gallagher, and Hertel[5]). The plane determined by these latter two vectors will be called the *collision (or scattering) plane*. The collision frame is associated with the inelastic process and is defined in such a way that its Z axis (Z_{col}) is along the momentum $\mathbf{k}_{\text{in}}$ (that is, along $-\mathbf{k}_f$) of the incident electron for this inelastic process. X_{col} is chosen to be in the collision plane and the positive X_{col} axis and $\mathbf{k}_{\text{out}}(=-\mathbf{k}_i)$ will be on the same side of the Z_{col} axis (i.e., the polar angles associated with the direction of scattered electron of the inelastic collision processes are $\phi_e = 0$ and $\theta_e \geq 0$). Y_{col} is chosen such that a right-handed coordinate system is obtained. The $[Z_{\text{col}}, X_{\text{col}}]$ plane will then be identical with the collision plane.

The Z axis of the photon frame (Z_{ph}) is chosen along the polarization vector $(\hat{e}_\nu)$ of the incident laser light. Under these conditions Eq. (9) holds. Since this is the only equation of importance to us, the choice of X_{ph} and Y_{ph} is completely arbitrary and cannot influence any of our results. Here, we will choose X_{ph} in the direction of the incoming laser light and Y_{ph} in such a way that the photon frame $[X_{\text{ph}}, Y_{\text{ph}}, Z_{\text{ph}}]$ becomes a right-handed coordinate system. The relative position of the photon frame to the collision frame can be characterized by giving the angle ψ of the vector $\hat{e}_\nu$ with respect to a *specified reference direction* as well as the polar angles of the direction of laser incidence $(\theta_{\hat{n}}, \phi_{\hat{n}})$ with respect to the collision frame.

In order to describe the experimental conditions and facilitate the transformation from the photon frame to the collision frame, a third coordinate system, called the *laser frame* (following Macek and Hertel) will be introduced whose axes will be denoted by $X_{\text{ph}'}$, $Y_{\text{ph}'}$, and $Z_{\text{ph}'}$. $Z_{\text{ph}'}$ will be selected along the laser line of incidence but against the direction of incidence (i.e., opposite direction to the positive X_{ph} axis). The polar angles of the positive $Z_{\text{ph}'}$ axis in the collision frame will be denoted by $\theta_{\hat{n}}$ and $\phi_{\hat{n}}$. The $X_{\text{ph}'}$ axis is chosen to lie in the $[Z_{\text{ph}'}, Z_{\text{col}}]$ plane in such a way that the laser frame $[X_{\text{ph}'}, Y_{\text{ph}'}, Z_{\text{ph}'}]$ is obtained from the collision frame $[X_{\text{col}}, Y_{\text{col}}, Z_{\text{col}}]$ through rotations by Euler angles[18] $\alpha = \phi_{\hat{n}}, \beta = \theta_{\hat{n}},$ and $\gamma = 0$. The positive $X_{\text{ph}'}$ axis will be chosen as the reference direction for $\hat{e}_\nu$, thus ψ will denote the angle between the $\hat{e}_\nu$ vector (i.e., the positive Z_{ph} axis) and the positive $X_{\text{ph}'}$ axis. The above selection of coordinate systems makes the transformations from one to the other extremely simple. It can be seen easily that the photon frame is obtained from the laser frame through rotations by Euler angles $\alpha = \psi, \beta = \pi/2,$ and $\gamma = 0$. Thus the transformation from the *collision frame* to the *laser frame* and from there to the *photon frame* has been fully described. The relationship among these three coordinate systems is shown in Fig. 1.

D. Formulas for the superelastic scattering intensity

Since according to Eq. (8) the superelastic scattering intensity depends on $\hat{\tau}$, and since according to Eq. (1) [and Eq. (9) as the special case of importance to us here] $\hat{\tau}$ can be expressed easily in the photon frame, it is our objective now to transform this expression into the collision frame. In order to do that, it is desirable that $\hat{\tau}$ be resolved into components of irreducible tensor operators whose transformation properties are well known and simple. The resolution of a density operator into its irreducible components was first proposed by Fano.[11] It can be shown that any operator, acting within the vector space determined by the basis vectors $|nJM_J\rangle$ with $J \geq M_J \geq -J$, can be expressed in terms of the components of irreducible tensor operators $\hat{\tau}_q^{[k]}$, and thus $\hat{\tau}$ can also be given by

$$\hat{\tau} = \sum_{kq} b_{kq} \hat{\tau}_q^{[k]} \, , \tag{10}$$
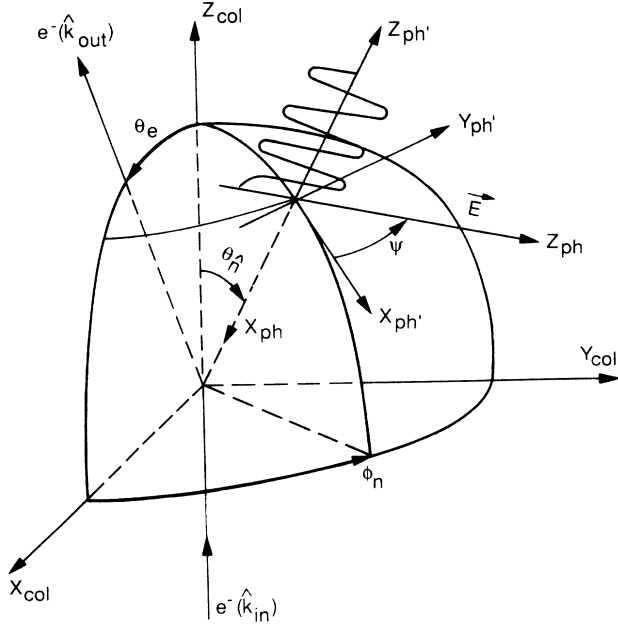
where

FIG. 1. The general definition of the col, ph, and ph' coordinate systems, the laser light propagation and linear polarization directions, and the incoming and scattered electron directions for the inelastic scattering process.

$$\hat{\tau}_q^{[k]} = \sum_{M_J', M_J''} |nJM_J'\rangle\langle nJM_J''|$$

$$\times (J - M_J''JM_J'|kq)(-1)^{k-J-M_J''} \quad (11)$$

is the qth component of an irreducible tensor operator of rank k. The b_{kq} coefficients can be calculated from

$$b_{kq} = \mathrm{tr}(\hat{\tau}\,\hat{\tau}_q^{[k]\dagger}) , \quad (12)$$

where $\hat{\tau}_q^{[k]\dagger}$ is the Hermitian adjoint of $\hat{\tau}_q^{[k]}$. The coefficients b_{kq} were called *statistical tensors* or *state mul-*

tipoles by Fano.[11] Equation (12) can be used to calculate these coefficients when $\hat{\tau}$ is given by Eq. (1) yielding

$$b_{kq} = \sum_{M_J} (kq|J - M_JJM_J)W(M_J)(-1)^{k-J-M_J} . \quad (13)$$

Evidently $b_{kq} = 0$ for $q \neq 0$ in our case since for $q \neq 0$ the Clebsch-Gordan coefficient in Eq. (13) is zero. Substituting Eq. (13) into Eq. (10) and the results, in turn, into Eq. (8), we get for the superelastic scattering intensity

$$I^S = \overline{C} \sum_k w(k)\langle \hat{\tau}_0^{[k]}(\mathrm{ph})\rangle , \quad (14)$$

where $w(k)$ is defined by

$$w(k) \equiv b_{k0} = \sum_{M_J} (-1)^{k-J-M_J} W(M_J)(J - M_JJM_J|k0) . \quad (15)$$

The expression $\hat{\tau}_0^{[k]}(\mathrm{ph})$ refers to the $\hat{\tau}_0^{[k]}$ operator defined in the photon frame. The $\hat{\tau}^{[k]}$ operator in the laser frame will be denoted by $\hat{\tau}^{[k]}(\mathrm{ph}')$ and in the collision frame by $\hat{\tau}^{[k]}(\mathrm{col})$. Similar notation will be used for other tensor operators. In the special case of interest to us, when $\hat{\tau}$ is given by Eq. (9), we obtain

$$W(1) = W(-1) = 0, \quad W(0) = 1 , \quad (16)$$

which gives for $w(k)$, via Eq. (15),

$$w(0) = \frac{1}{\sqrt{3}}, \quad w(1) = 0, \quad w(2) = -\sqrt{2/3} . \quad (17)$$

Substituting these expressions into Eq. (14), one obtains, for the superelastic scattering intensity,

$$I^S = \overline{C}\left[\frac{1}{\sqrt{3}}\langle \hat{\tau}_0^{[0]}(\mathrm{ph})\rangle - \sqrt{2/3}\langle \hat{\tau}_0^{[2]}(\mathrm{ph})\rangle\right] . \quad (18)$$

Using the definitions and the transformation formulas of the $\hat{T}_{qp}^{[k]}$ ($q = 0,1,2$ and $p = +$ or $-$) tensor operators of Macek and Hertel,[10] we arrive at the following expression for the superelastic scattering intensity:

$$I^S = \frac{\overline{C}}{3}\left\{1 + \tfrac{1}{4}(3\cos^2\theta_{\hat{n}} - 1)\langle \hat{T}_{0+}^{[2]}(\mathrm{col})\rangle + \frac{\sqrt{3}}{2}\sin\theta_{\hat{n}}\cos\theta_{\hat{n}}\cos\phi_{\hat{n}}\langle \hat{T}_{1+}^{[2]}(\mathrm{col})\rangle + \frac{\sqrt{3}}{4}\sin^2\theta_{\hat{n}}\cos2\phi_{\hat{n}}\langle \hat{T}_{2+}^{[2]}(\mathrm{col})\rangle\right.$$

$$-\frac{\sqrt{3}}{2}\cos2\psi\left[\frac{\sqrt{3}}{2}\sin^2\theta_{\hat{n}}\langle \hat{T}_{0+}^{[2]}(\mathrm{col})\rangle - \cos\phi_{\hat{n}}\sin\theta_{\hat{n}}\cos\theta_{\hat{n}}\langle \hat{T}_{1+}^{[2]}(\mathrm{col})\rangle + \left[1 - \frac{\sin^2\theta_{\hat{n}}}{2}\right]\cos2\phi_{\hat{n}}\langle \hat{T}_{2+}^{[2]}(\mathrm{col})\rangle\right]$$

$$\left. -\frac{\sqrt{3}}{2}\sin2\psi[\sin\phi_{\hat{n}}\sin\theta_{\hat{n}}\langle \hat{T}_{1+}^{[2]}(\mathrm{col})\rangle - \sin2\phi_{\hat{n}}\cos\theta_{\hat{n}}\langle \hat{T}_{2+}^{[2]}(\mathrm{col})\rangle]\right\} . \quad (19)$$

I^S can also be given in terms of the EICP of da Paixão et al. for the excitation of a $J = 1$ state.[14] We will follow the latter course with the definitions[19]

$$\langle \hat{T}_{0+}^{[2]}(\mathrm{col})\rangle = 1 - 3\lambda , \quad (20a)$$

$$\langle \hat{T}_{1+}^{[2]}(\mathrm{col})\rangle = 2\sqrt{3}[\lambda(1-\lambda)]^{1/2}\cos\tilde{\chi}\cos\Delta$$

$$= 2\sqrt{3}[\lambda(1-\lambda)]^{1/2}\cos\chi , \quad (20b)$$

$$\langle \hat{T}_{2+}^{[2]}(\mathrm{col})\rangle = \sqrt{3}(\lambda - 1)\cos\epsilon . \quad (20c)$$

The general expression for the superelastic scattering intensity is then

$$I^S \sim A + B'\cos2\psi + B''\sin2\psi , \quad (21)$$

where

$$A = 1 + \tfrac{1}{4}(1-3\lambda)(3\cos^2\theta_{\hat{n}} - 1)$$

$$+ \tfrac{3}{2}\sqrt{\lambda(1-\lambda)}\cos\tilde{\chi}\cos\Delta\sin2\theta_{\hat{n}}\cos\phi_{\hat{n}}$$

$$+ \tfrac{3}{4}(\lambda - 1)\cos\epsilon\sin^2\theta_{\hat{n}}\cos2\phi_n , \quad (22)$$

$$B' = -\tfrac{3}{4}\sin^2\theta_\hbar(1-3\lambda)$$

$$+ 3\sin\theta_\hbar\cos\theta_\hbar\cos\phi_\hbar\sqrt{\lambda(1-\lambda)}\cos\tilde{\chi}\cos\Delta$$

$$-\tfrac{3}{2}(1-\tfrac{1}{2}\sin^2\theta_\hbar)\cos2\phi_\hbar(\lambda-1)\cos\epsilon , \qquad (23)$$

$$B'' = -3\sin\phi_\hbar\sin\theta_\hbar\sqrt{\lambda(1-\lambda)}\cos\tilde{\chi}\cos\Delta$$

$$+\tfrac{3}{2}\sin2\phi_\hbar\cos\theta_\hbar(\lambda-1)\cos\epsilon . \qquad (24)$$

III. MODELING CALCULATIONS

A. Coordinate systems

The dimensions of the extended scattering volume are defined by the overlap of the detector view cone, the electron beam, the atomic beam, and (for superelastic scattering studies) the laser beam. Modeling is carried out by representing this extended volume as an array of discrete scattering centers, applying the theoretical formalism to each center, and performing a weighted average of the
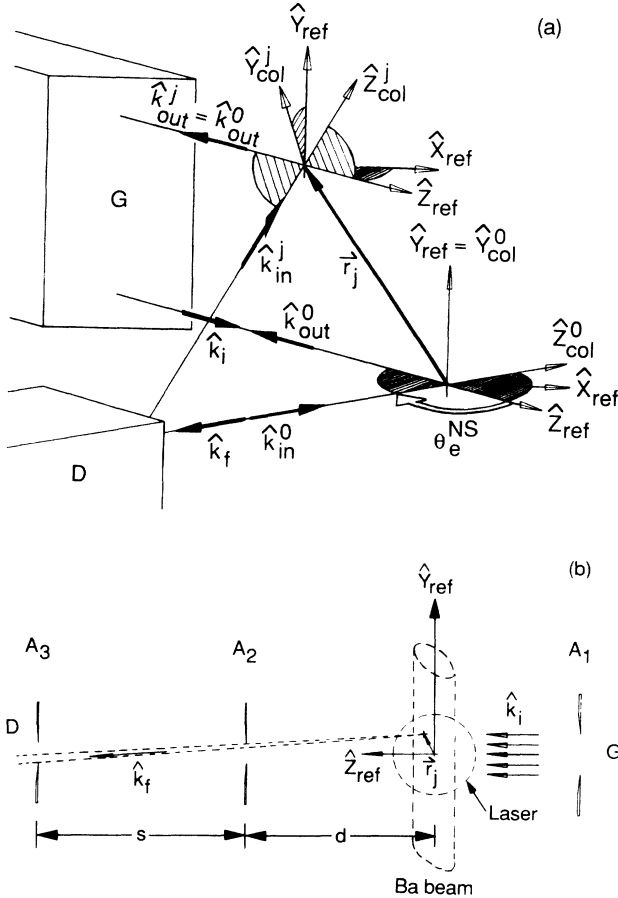

FIG. 2. (a) Schematic diagram showing the relationship among the various coordinate frames and momentum vectors. See text for definitions and explanations. G and D refer to the gun and detector, respectively. (b) Schematic diagram of the scattering geometry and the pertinent dimensions (in cm) of our experimental apparatus. The electron momentum vectors for the superelastic scattering have been indicated. $A_1 = 0.305$, $A_2 = A_3 = 0.127$, $s = 1.52$, and $d = 1.36$ cm. The Ba beam and laser beam diameters are 0.1 and 0.3 cm, respectively.

contributions. To this end, a coordinate system, which we call the *laboratory or reference frame,* is defined and fixed to the apparatus [see Figs. 2(a) and 2(b)]. This laboratory frame is determined by optical alignment of the electron gun, detector, and target beam axes. Proper alignment of these three components ensures that a plane can be defined in which the gun and detector axes will lie as the detector is rotated. The laboratory frame is tied to the apparatus as follows. The direction of the incident electron beam (assumed to be parallel with the axis of the electron gun) defines the $Z_{\rm ref}$ axis. The $X_{\rm ref}$ axis is chosen to lie within the plane defined by the gun and detector axes such that the positive $X_{\rm ref}$ direction points "left" from the point of view of an electron emitted by the gun. The $Y_{\rm ref}$ axis is fixed by the requirement of a right-handed coordinate system (i.e., $\hat{Y}_{\rm ref}=\hat{Z}_{\rm ref}\times\hat{X}_{\rm ref}$, where $\hat{X}_{\rm ref}$ refers to a unit vector in the direction of the positive $X_{\rm ref}$ axis and similarly for $Y_{\rm ref}$ and $Z_{\rm ref}$). In our experimental arrangement, $\hat{Y}_{\rm ref}$ coincides with the atomic beam axis and points vertically upwards. For an ideal, single-point collision occurring at the origin of the laboratory frame, the momentum vectors $\mathbf{k}_i$ and $\mathbf{k}_f$ lie in the plane defined by the gun and detector axes and we therefore refer to this plane as the *nominal scattering plane.* We can define a *nominal scattering angle* $\theta_e^{\rm ns}$, as the angle between $\mathbf{k}_i$ and $\mathbf{k}_f$ for this ideal scattering event at the origin. This angle is referred to as "nominal" in the sense that it is defined by the angular difference between the electron gun and detector axes. *True scattering angles* corresponding to a collision at some arbitrary point within the extended scattering volume will, generally, not be identical to the nominal angle. We arbitrarily label $\theta_e^{\rm ns}$ with a positive or negative sign depending on whether the electron is superelastically scattered to the left or right from the viewpoint of the incident electron.

The laser incidence vector $\mathbf{k}_v$ and polarization vector $\hat{\epsilon}_v$ can be expressed in terms of the nominal laser beam polar angles and nominal linear polarization direction in the laboratory frame (denoted by θ_v, ϕ_v, and ψ_v). The incident vector is given by

$$\hat{\mathbf{k}}_v = -\hat{X}_{\rm ref}\sin\theta_v\cos\phi_v - \hat{Y}_{\rm ref}\sin\theta_v\sin\phi_v - \hat{Z}_{\rm ref}\cos\theta_v . \qquad (25)$$

Note that $\hat{\mathbf{k}}_v = -\hat{Z}_{\rm ph'}$ as discussed in Sec. II. The polarization vector is given by

$$\hat{\epsilon}_v = \hat{X}_{\rm ref}(\cos\psi_v\cos\theta_v\cos\phi_v - \sin\psi_v\sin\phi_v)$$

$$+ \hat{Y}_{\rm ref}(\cos\psi_v\cos\theta_v\sin\phi_v + \sin\psi_v\cos\phi_v)$$

$$+ \hat{Z}_{\rm ref}\cos\psi_v\sin\theta_v . \qquad (26)$$

For $\psi_v = 0$ and $\phi_v = 0$, $\hat{\epsilon}_v$ lies in the nominal scattering plane $[X_{\rm ref}, Z_{\rm ref}]$.

The theoretical formalism developed in Sec. II expresses the superelastic scattering intensity in terms of laser polar angles $\theta_\hbar$, $\phi_\hbar$, and ψ as measured in a collision frame, which in turn is defined by the incident and scattered electron momentum vectors associated with the time-inverse inelastic scattering event occurring at a particular scattering point. In order to apply this formalism

to the more general treatment of an extended scattering volume, we must generalize the notation somewhat and introduce the superscript j to distinguish a collision event occurring at the jth scattering center, which is characterized by the position vector $\mathbf{r}_j$ in the reference frame. The electron momenta are written as $\mathbf{k}_{\text{in}}^j$ and $\mathbf{k}_{\text{out}}^j$ for this scattering event. The true laser angles, as measured in the jth collision frame, become $\theta_{\hat{n}}^j$, $\phi_{\hat{n}}^j$, and ψ^j. The true scattering angle in this frame is also generally different than the nominal scattering angle and we denote it as θ_e^j. In some cases, we will refer to an "ideal" scattering event taking place at the reference frame origin (i.e., $\mathbf{r}_j = 0$). A zero superscript (i.e., $j=0$) will denote such a scattering event. The unit vectors along the momenta of the incident and scattered electrons in the ideal inelastic process can be written in terms of reference frame coordinates

$$\mathbf{k}_{\text{in}}^0 = -\sin\theta_e^{\text{ns}}\hat{\mathbf{X}}_{\text{ref}} - \cos\theta_e^{\text{ns}}\hat{\mathbf{Z}}_{\text{ref}} ,$$

$$\hat{\mathbf{k}}_{\text{out}}^0 = -\hat{\mathbf{Z}}_{\text{ref}} . \tag{27}$$

The transformation from nominal laser angles θ_v, ϕ_v, and ψ_v and nominal scattering angle θ_e^{ns} to the "true" angles associated with the collision frame of the "ideal" scattering event (i.e., $\theta_{\hat{n}}^0$, $\phi_{\hat{n}}^0$, ψ^0, and θ_e^0) is relatively simple:

$$\theta_e^0 = |\theta_e^{\text{ns}}| ,$$

$$\cos\theta_{\hat{n}}^0 = \hat{\mathbf{Z}}_{\text{ph}} \cdot \hat{\mathbf{k}}_{\text{in}}^0 \tag{28}$$

$$\phi_{\hat{n}}^0 = \phi_v .$$

The only ambiguity arises for $\phi_v = 0$ in which case $\phi_{\hat{n}}^0$ is determined by the following considerations:

$$\phi_{\hat{n}}^0 = 0 \quad \text{for} \quad -\pi < \theta_e^{\text{ns}} < -\theta_v ,$$

$$\phi_{\hat{n}}^0 = \pi \quad \text{for} \quad -\theta_v < \theta_e^{\text{ns}} < 0 ,$$

$$\phi_{\hat{n}}^0 = 0 \quad \text{for} \quad 0 < \theta_e^{\text{ns}} < \pi - \theta_v , \tag{29}$$

$$\phi_{\hat{n}}^0 = \pi \quad \text{for} \quad \pi - \theta_v < \theta_e^{\text{ns}} < \pi .$$

For the case of $\phi_v = 0$, we obtain the simple relationship for $\theta_{\hat{n}}^0$,

$$\theta_{\hat{n}}^0 = \theta_v + \theta_e . \tag{30}$$

The transformation from nominal angles θ_v, ϕ_v, ψ_v and θ_e^{ns} in the reference frame, to true angles $\theta_{\hat{n}}^j$, $\phi_{\hat{n}}^j$, ψ^j, and θ_e^j in the collision frame, whose origin is located at some arbitrary position vector $\mathbf{r}_j$, is more difficult and exhibits a complicated dependence on the nominal scattering angle, θ_e^{ns}. However, a straightforward determination of this transformation is accomplished by expressing the general unit vectors $\hat{\mathbf{k}}_{\text{in}}^j = \mathbf{k}_{\text{in}}^j / |\mathbf{k}_{\text{in}}^j|$ and $\hat{\mathbf{k}}_{\text{out}}^j = \mathbf{k}_{\text{out}}^j / |\mathbf{k}_{\text{out}}^j|$ in terms of the "ideal scattering" momentum vectors $\hat{\mathbf{k}}_{\text{in}}^0$ and $\hat{\mathbf{k}}_{\text{out}}^0$. For a given $\hat{\mathbf{k}}_{\text{in}}^0$ and $\hat{\mathbf{k}}_{\text{out}}^0$, the range of possible vectors $\hat{\mathbf{k}}_{\text{in}}^j$ and $\hat{\mathbf{k}}_{\text{out}}^j$ giving rise to the detection of a collision event is determined by the details of the model. This is described further in Sec. III D. For the present discussion, however, we concentrate on a simple model in which electron detection occurs at a single point located

on the detector axis at a distance of r_{det} from the laboratory frame origin. In this case,

$$\hat{\mathbf{k}}_{\text{in}}^j = (r_{\text{det}}\hat{\mathbf{k}}_{\text{in}}^0 + \mathbf{r}_j)/|r_{\text{det}}\hat{\mathbf{k}}_{\text{in}}^0 + \mathbf{r}_j| ,$$

$$\hat{\mathbf{k}}_{\text{out}}^j = \hat{\mathbf{k}}_{\text{out}}^0 . \tag{31}$$

The relationship between $\hat{\mathbf{k}}_{\text{out}}^j$ and $\hat{\mathbf{k}}_{\text{out}}^0$ holds under the assumption of a parallel incoming electron beam in the superelastic scattering experiment. The true scattering angle for a collision occurring at $\mathbf{r}_j$ is given by

$$\cos\theta_e^j = \hat{\mathbf{k}}_{\text{in}}^j \cdot \hat{\mathbf{k}}_{\text{out}}^j . \tag{32}$$

The coordinate axes of the true collision frame at this scattering center are

$$\hat{\mathbf{Z}}_{\text{col}} = \hat{\mathbf{k}}_{\text{in}}^j ,$$

$$\hat{\mathbf{Y}}_{\text{col}} = \hat{\mathbf{k}}_{\text{in}}^j \times \hat{\mathbf{k}}_{\text{out}}^j , \tag{33}$$

$$\hat{\mathbf{X}}_{\text{col}} = \hat{\mathbf{Y}}_{\text{col}} \times \hat{\mathbf{Z}}_{\text{col}} .$$

For the sake of clarity in the presentation, no j superscripts have been appended to the collision frame axes, although it is apparent from their definition that they are j dependent.

We now determine the true laser angles $\theta_{\hat{n}}^j$, $\phi_{\hat{n}}^j$, and ψ^j in this collision frame. The laser angle $\theta_{\hat{n}}^j$ is given by the dot product

$$\cos\theta_{\hat{n}}^j = \hat{\mathbf{Z}}_{\text{ph}'} \cdot \hat{\mathbf{Z}}_{\text{col}} . \tag{34}$$

The laser azimuthal angle ϕ_n^j is determined by

$$\cos\phi_n^j = (\hat{\mathbf{Z}}_{\text{col}} \times \hat{\mathbf{Z}}_{\text{ph}'}) \cdot \hat{\mathbf{Y}}_{\text{col}} . \tag{35}$$

Since this expression defines ϕ_n^j in terms of a cosine, it cannot give the sign of ϕ_n^j. For a complete description of ϕ_n^j, the sign is required and is given by the projection of $\hat{\mathbf{Z}}_{\text{ph}'}$ on $\hat{\mathbf{Y}}_{\text{col}}$,

$$\phi_n^j > 0 \quad \text{for} \quad \hat{\mathbf{Z}}_{\text{ph}'} \cdot \hat{\mathbf{Y}}_{\text{col}} > 0 ,$$

$$\phi_n^j < 0 \quad \text{for} \quad \hat{\mathbf{Z}}_{\text{ph}'} \cdot \hat{\mathbf{Y}}_{\text{col}} < 0 . \tag{36}$$

Note that this determination of sign is necessary for ϕ_n^j because it can vary from 0 to 2π or, equivalently, from $-\pi$ to π. The angles θ_e^j and θ_n^j do not require a sign determination because they vary from 0 to π and are uniquely defined by the cosine.

The transformed polarization angle ψ^j is obtained as follows. First, the photon frame coordinate axes are found:

$$\hat{\mathbf{Z}}_{\text{ph}'} = -\hat{\mathbf{k}}_v ,$$

$$\hat{\mathbf{Y}}_{\text{ph}'} = -\hat{\mathbf{Z}}_{\text{col}} \times \hat{\mathbf{Z}}_{\text{ph}'} , \tag{37}$$

$$\hat{\mathbf{X}}_{\text{ph}'} = \hat{\mathbf{Y}}_{\text{ph}'} \times \hat{\mathbf{Z}}_{\text{ph}'} .$$

Once again, for the sake of clarity, no j superscript has been attached to $\hat{\mathbf{X}}_{\text{ph}'}$ or $\hat{\mathbf{Y}}_{\text{ph}'}$, although they are both j dependent. Note that $\hat{\mathbf{Z}}_{\text{ph}'}$ is j independent under the assumption of an incoming parallel laser beam. The angle ψ^j is then given by

$$\cos\psi^j = \hat{\epsilon}_v \cdot \hat{X}_{ph'} \ . \tag{38}$$

A sign is also assigned to ψ^j since $\hat{\epsilon}_v$ can rotate through 2π rad (or from $-\pi$ to π rad). Of course, any functional dependence on ψ^j will reflect the fact that ψ^j and $\psi^j + \pi$ are equivalent. The sign is chosen as follows:

$$\psi^j > 0 \quad \text{for} \ \hat{\epsilon}_v \cdot \hat{Y}_{ph'} < 0$$
$$\psi^j < 0 \quad \text{for} \ \hat{\epsilon}_v \cdot \hat{Y}_{ph'} > 0 \ . \tag{39}$$

The relationship between any of the nominal laser angles and their counterparts for an offset scatterer would be difficult to express analytically. The same applies to the nominal and true scattering angles. The computer code evaluates all the relevant vector products directly in order to extract the true laser and scattering angles at each nominal scattering angle. These true angles are then substituted into Eq. (21) for the evaluation of the superelastic scattering intensity. To carry out modeling calculations, we adopted the geometry shown in Figs. 2(a) and 2(b), which closely corresponds to that of Register et al.[7] and the present experiments. We assume that, at the interaction region, the incident electron beam is parallel, as is the laser beam.

Figures 3(a)–3(d) show the variation of θ_e^0, $\theta_{\hat{n}}^0$, $\phi_{\hat{n}}^0$, and $\delta\psi^0(=\psi^0-\psi_v)$ for the ideal scattering event (i.e., $r_j=0$) as well as the variation of θ_e^j, $\theta_{\hat{n}}^j$, $\phi_{\hat{n}}^j$, and $\delta\psi^j(=\psi^j-\psi_v)$ for a point offset vertically by $\mathbf{r}_j = r_j \hat{Y}_{ref}$, where $r_j = 0.12$ cm. For these angle transformations we determine the direction of $\hat{k}_{out}^j$ by fixing it along a ray which connects the scattering point to the center of the detector aperture located at $r_{det} = s + d = 2.88$ cm away from the nominal scattering center [see Fig. 2(b)]. Remembering that $\hat{k}_{out}^j = -\hat{Z}_{ref}$, we find that a vertical offset of 0.12 cm implies an angular offset of 2.4°. For a point offset symmetrically to the opposite side of the nominal scattering plane (i.e., $\mathbf{r}_j = r_j \hat{Y}_{ref}$, where $r_j = -0.12$ cm), θ_e^j and $\theta_{\hat{n}}^j$ remain unchanged while $\phi_{\hat{n}}^j$ and $\delta\psi^j$ change sign. For an offset scattering point (i.e., for $j \neq 0$), θ_e^j never reaches the zero value and its deviation from zero at $\theta_e^{ns} = 0$ depends on the magnitude of the offset. [In Fig. 3(a), for the vertical offset of $\mathbf{r}_j = 0.12$ cm $\hat{Y}_{ref}$, the value of θ_e^j at $\theta_e^{ns} = 0$, is given by the angular offset, i.e., 2.4°.] The true laser polar angle $\theta_{\hat{n}}^j$ (for arbitrary j) changes linearly with θ_e^{ns} except in the regions where the detector crosses the laser beam. In this region, a slight deviation from linearity is noted for $j=0$ [Fig. 3(b)]. The laser azimuthal angle $\phi_{\hat{n}}^j$ undergoes large changes near $\theta_e^{ns} = 0$, $-\theta_v$, and $\pi - \theta_v$, For $j=0$, these changes occur discontinuously by π rad in agreement with the transformation equations (29). Although these changes seem drastic, we will show below that they do not have an observable effect on the superelastic scattering intensity. For $j \neq 0$ (i.e., for an offset scatterer) the behavior of $\phi_{\hat{n}}^j$ differs significantly from that of $\phi_{\hat{n}}^0$. The large changes near $\phi_e^{ns} = 0$, $-\theta_v$, and $\pi - \theta_v$ occur more slowly with θ_e^{ns}, implying that $\phi_{\hat{n}}^j$ can assume a range of values from 0 to π near these critical nominal scattering angles. Note also that the difference

between $\phi_{\hat{n}}^j$ and $\phi_{\hat{n}}^0$ persists over relatively large regions of θ_e^{ns}. Our modeling results show (see below) that this slower variation of $\phi_{\hat{n}}^j$ with θ_e^{ns}, as opposed to the discontinuous variation of $\phi_{\hat{n}}^j$, is partly responsible for dramatic effects in the measured superelastic scattering intensity. This can be further understood by reference to the expression for superelastic scattering intensity [Eq. (21)]. Examination of this equation shows that it is identical for the cases $\phi_{\hat{n}} = 0$ and π. Therefore a discontinuous change in $\phi_{\hat{n}}$ from 0 to π does not affect the observed superelastic intensity while, for a slower (nondiscontinuous) change, this equation definitely changes in accordance with the functional dependence on $\phi_{\hat{n}}$. An idealized physical example can be given which illustrates these effects. At $\theta_e^{ns} = 0+$ (where the plus sign indicates a small positive angle), a scattering event occurring at a point vertically offset from the nominal scattering plane defines a true scattering plane nearly perpendicular to the nominal scattering plane. The ideal scattering even occurs for $\phi_{\hat{n}}^0 = 0$ while the offset scattering event occurs for $\phi_{\hat{n}}^j$ nearly equal to $\pi/2$. Thus a completely different experimental geometry is defined in the offset scattering case. As the nominal scattering angle is increased, the true scattering plane, defined by a collision at this offset point, slowly twists into near alignment with the nominal scattering plane until the next critical angle of $\theta_e^{ns} = \pi - \theta_v$ is approached. Although it is clear that a problem exists at near-zero nominal scatteing angles and, likewise, at the other critical nominal scattering angles, we have discovered that strong geometry-related effects on the superelastic scattering intensity can manifest themselves in the region between these critical angles. This is due to the complex interplay between the behavior of the scattering geometry for an offset scatterer and the behavior of the coherence parameters with scattering angle. We discuss this in more detail in Sec. III B.

Figure 3(d) shows the deviation ($\delta\psi^j$) between ψ^j and ψ_v as a function of θ_e^{ns}. The behavior of $\delta\psi^0$ shows discontinuous changes by π at $\theta_e^{ns} = -\theta_v$ and $\pi - \theta_v$, while, for an offset scatterer, $\delta\psi^j$ varies more slowly through these critical angles. We can again argue that the discontinuous changes in $\delta\psi^0$ are "unseen" by a superelastic scattering signal measurement. The polarization angle ψ enters Eq. (24) through the terms $\cos(2\psi)$ and $\sin(2\psi)$ which become, when applied to the ideal scattering event under discussion, $\cos(2\psi^0)$ and $\sin(2\psi^0)$. However,

$$\cos(2\psi^0) = \cos(2\psi_v + 2\delta\psi^0) \ ,$$
$$\sin(2\psi^0) = \sin(2\psi_v + 2\delta\psi^0) \ . \tag{40}$$

Clearly, for a discontinuous jump in $\delta\psi^0$ by π rad, there will be a corresponding discontinuous jump in $2\delta\psi^0$ by 2π rad which leaves the sine and cosine functions unchanged. Once again, as in the case of $\phi_{\hat{n}}^j$, it is the deviation from discontinuous behavior that can lead to observable effects in I^S.
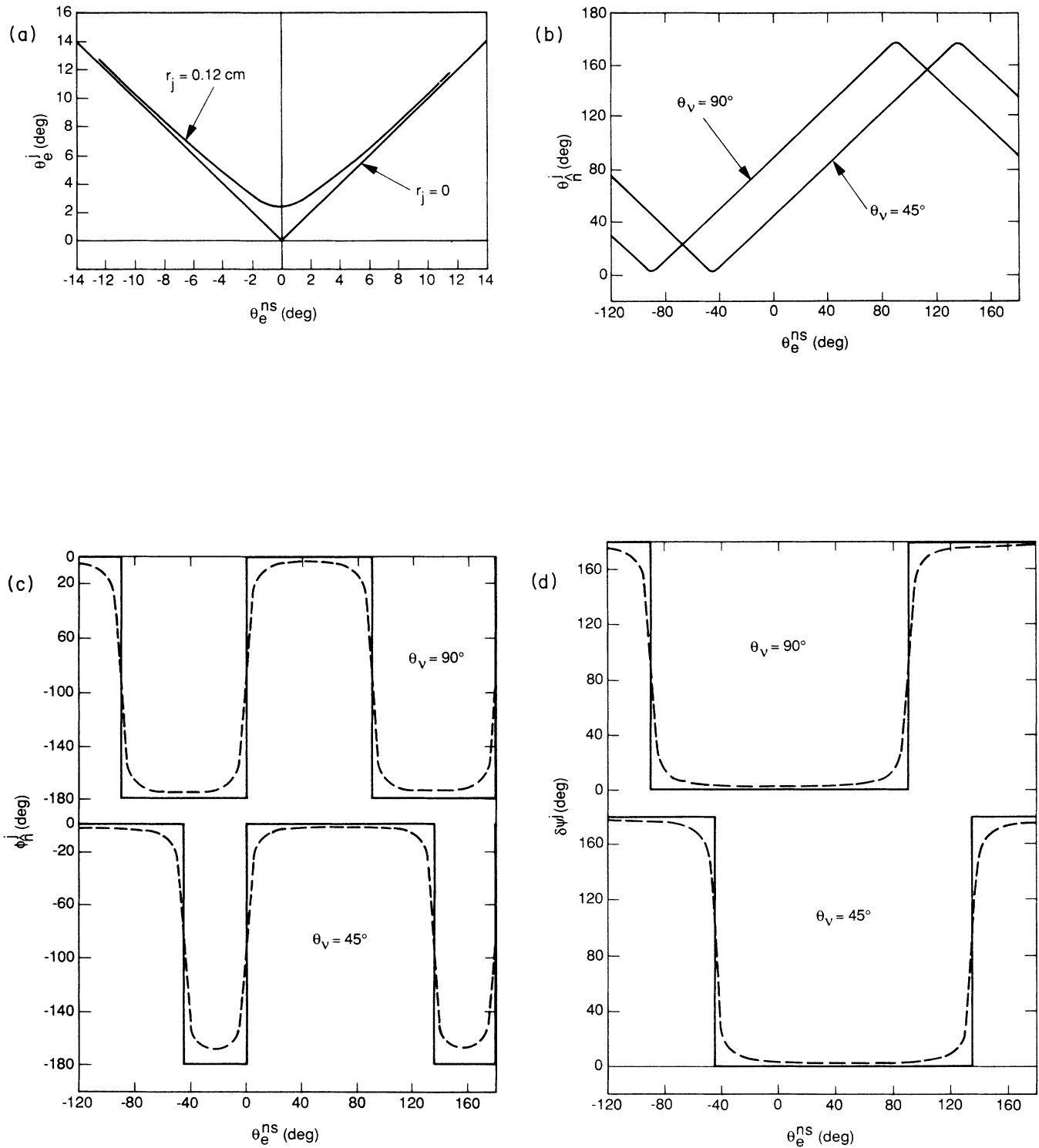
FIG. 3. (a) Variation of the true scattering angle θ_e^j with θ_e^{ns} for a scattering point located at $\mathbf{r}_j = r_j \hat{\mathbf{Y}}_{ref}$ ($r_j = 0.12$ cm) and for a scattering point at the origin of the laboratory coordinate frame indicated as $r_j = 0$. (b) Variation of the true laser polar angle (θ_e^j) with θ_e^{ns} for a scattering point located at $\mathbf{r}_j = r_j \hat{\mathbf{Y}}_{ref}$ ($r_j = 0.12$ cm) and for two laser configurations as indicated. In both cases the laser beam is in the nominal scattering plane. (c) Variation of true laser azimuthal angle (ϕ_n^j) for scattering points located at $\mathbf{r}_j = r_j \hat{\mathbf{Y}}_{ref}$ with $r_j = 0$ and 0.12 cm as indicated by solid and dashed lines, respectively. The upper curves refer to laser geometry of $\theta_v = 90°$ and the lower ones to $\theta_v = 45°$. (d) Variation of $\delta\psi^j = (\psi^j - \psi_v)$ for scattering points located at $r_j = 0$ and 0.12 cm as indicated by solid and dashed lines, respectively. The upper and lower curves correspond to $\theta_v = 90°$ and 45°, respectively.

B. Modeling calculations

To facilitate the modeling, Eq. (21) was rewritten as

$$I_j^S(\psi^j) \sim 1 + \eta^j \cos(2\psi^j + 2\alpha^j) \ , \tag{41}$$

where we define the modulation depth to be

$$\eta^j = (B_j'^2 + B_j''^2)^{1/2}/A_j \tag{42}$$

and the modulation phase shift to be

$$\alpha^j = \tfrac{1}{2}\tan^{-1}(-B_j''/B_j') \ . \tag{43}$$

The superelastic scattering intensity I_j^S carries the subscript j since it arises from scattering at the jth scattering center. The quantities A, B', and B'' as defined in Eq. (21) are also subscripted by j since they are now functions of the true laser angles and scattering angles in the collision frame corresponding to the jth scattering center (i.e., $\theta_{\hat{n}}^j$, $\phi_{\hat{n}}^j$, and θ_e^j). Equation (41) is not written in the most convenient form since the functional dependence is on ψ^j, which changes with collision frame. It is better expressed as

$$I_j^S(\psi_v) \sim 1 + \eta^j \cos(2\psi_v + 2\delta\psi^j + 2\alpha^j) \ , \tag{44}$$

where ψ_v is the experimentally adjustable quantity. Equation (44) gives the superelastic scattering signal intensity arising from a single scatterer, located relative to the reference frame origin by position vector $\mathbf{r}_j$, as a function of the nominal laser polarization angle ψ_v. Written in this form, Eq. (44) can be seen to contain two sources of phase shift. The α^j term arises from the sine term in Eq. (21). For the case of $\phi_{\hat{n}}^j = 0$ or π, the B_j'' coefficient of this sine term vanishes and the phase shift α^j also vanishes. The $\delta\psi^j$ term comes about as a result of the collision frame dependence of the true polarization angle ψ^j. For an ideal scattering event (i.e., $j=0$) and $\phi_v=0$, this source of the phase shift vanishes. The characteristics of $\delta\psi^j$ have been discussed in detail in Sec. III A. We can define a total phase shift by

$$\alpha_{\text{tot}}^j = \alpha^j + \delta\psi^j \ . \tag{45}$$

For the purpose of extracting coherence parameters, η^j and α_{tot}^j completely specify the polarization dependence of the superelastic scattering intensity. Although it would also give useful information, the absolute measurement of I^S is prohibitively difficult. Our modeling calculations are therefore concerned with determining the behavior of the modulation depth η^j and the phase shift α_{tot}^j as a function of θ_e^{ns}.

The concept of a phase shift in the modulation was introduced empirically by Register et al.[7] to quantify an observed asymmetry of superelastic signal with respect to the (nominal) scattering plane in their measurements. The link between this phase shift and a nonvanishing sine term in Eq. (21) was made in that work, but the effect that caused this term to be nonzero was not clearly recognized despite exhaustive experimental tests. In the present treatment of scattering from an offset scattering center, we have introduced a priori the phase shift associated with the sine term (α^j) because of the realization

that the true laser polar angles as they appear in the jth collision frame may differ substantially from the laser polar angles in the $j=0$ collision frame associated with an ideal scattering event.

The formalism developed in Sec. II contains four EICP and is applicable to scattering processes where spin-orbit-coupling effects are important. The recent calculations of Clark et al.,[8] however, show that, for excitation of the ^{138}Ba($6s6p\ ^1P_1$) state, spin-orbit-coupling effects are negligible and $\cos\epsilon = \cos\Delta = 1$. Therefore only λ and χ parameters are used in the modeling calculations. We have employed λ and χ values calculated by Clark et al. for inelastic impact energies of 7.24, 12.24, 32.24, and 102.24 eV. These inelastic impact energies correspond to the superelastic impact energies ($E_0^s = E_0 - 2.24$ eV) of 5, 10, 30, and 100 eV in our superelastic electron scattering experiments, which will be described later.

C. Single-scattering-point results

As a first step in describing scattering from an extended volume we present results [Figs. 4(a)–4(d)] for the behavior of η_j and α_{tot}^j as a function of nominal scattering angle for a single-point scatterer located at $\mathbf{r}_j$ from the reference frame origin. All calculations were carried out for the scattering arrangement shown in Figs. 2(a) and 2(b). The offset vector was chosen to lie along the $\hat{\mathbf{Y}}_{\text{ref}}$ axis (i.e., $\mathbf{r}_j = r_j \hat{\mathbf{Y}}_{\text{ref}}$) since vertical displacements from the nominal scattering plane were found to be responsible for the salient aspects of the observed behavior. Coherence parameters (λ and χ) corresponding to $E_0 = 7.24$ eV impact energy were chosen for these calculations. The functional dependence of η^j and α_{tot}^j on θ_e^{ns} is shown for various vertical offsets, and for two laser positions $\phi_v = 0°$, $\theta_v = 45°$, and $\phi_v = 0°$, $\theta_v = 90°$.

Some significant observations can be made about the single-point modeling results. We found that for $\theta_v = 45°$ the total phase shift α_{tot}^j does not exhibit any large variation near the critical angle $\theta_e^{\text{ns}} = -45°$ [not shown in Fig. 4(a)]. We have seen in the preceding section, however, that, at the critical angle $\theta_e^{\text{ns}} = \theta_v$, $\delta\psi^j$ undergoes an excursion through 180°. This implies that α^j must change in such a way as to nearly cancel the $\delta\psi^j$ contribution in the region near $\theta_e^{\text{ns}} = \theta_v$. This effect is tied to the variation of $\phi_{\hat{n}}^j$, which also undergoes a swing through 180° near the critical angles of θ_e^{ns}. The degree of cancellation depends on the behavior of the coherence parameters in this region.

The calculations also show that the total phase shift remains the same in magnitude but changes sign for scattering centers offset equidistantly above or below the nominal scattering plane. This implies that the overall phase shift will disappear for a scattering volume symmetrically distributed with respect to the nominal scattering plane. This is discussed further when we examine the modeling of an extended source. We also find that the modulation depth behavior is identical for scattering points symmetrically located above and below the nominal scattering plane. The geometry-induced variation in modulation depth will thus persist for a symmetrically distributed scattering volume. In fact, by considerations

elaborated upon below, the modulation depth behavior will be exaggerated by a finite volume of scatterers, symmetrically or asymmetrically distributed.

For ideal scattering with laser beam in the nominal scattering plane (i.e., $\phi_v = 0$) we find that $\alpha^0 = 0$ for all nominal scattering angles. This can be quickly seen by noting that, for ideal scattering, $\phi_v = 0$ implies $\phi_{\hat{n}}^0 = 0$ or π, which subsequently implies $B_0'' = 0$ and therefore $\alpha^0 = 0$. For ideal scattering, laser beam in the nominal scattering plane, and coherence parameters evaluated under the assumption of LS coupling, we obtain $\eta^0 = 1$ for all nominal scattering angles. This can be quickly proved by noting that Eq. (21) yields

$$A_j - B_j' = \tfrac{3}{2}(1-\lambda)(1-\cos2\phi_{\hat{n}}^j \cos\epsilon) . \qquad (46)$$

For the ideal scattering event and $\phi_v = 0$, we have $\phi_{\hat{n}}^0 = 0$ or π, which gives

$$A_0 - B_0' = \tfrac{3}{2}(1-\lambda)(1-\cos\epsilon) . \qquad (47)$$

In the absence of spin-orbit-coupling effects $\cos\epsilon = 1$,

which gives $A_0 = B_0'$ and hence $\eta^0 = 1$ (since $B'' = 0$).

We find [Figs. 4(a)–4(d)] that the dramatic behavior of α_{tot}^j and η^j does not necessarily occur where the drastic change in $\phi_{\hat{n}}^j$ occurs (near $\theta_e^{ns} = 0$). The effect of an offset geometry can be significant at angles far from the critical θ_e^{ns}. Even for small offsets (0.2 mm or 0.4° angular offset) the phase shift for the $\theta_v = 45°$ configuration goes through 180° change at $\theta_e^{ns} = -10°$. The sharpness of this transition is a function of the magnitude of the offset of the scattering points [Fig. 4(a)]. The drastic change in the modulation depth arising from geometrical effects occurs at the same nominal scattering angle as the change in the phase shift [Fig. 4(b)]. For the $\theta_v = 90°$ laser configuration, the laser changes in the overall phase shift and modulation depth occur symmetrically at $\pm20°$ nominal scattering angle [Figs. 4(c) and 4(d)].

The scattering angle location of these dramatic features depends on the behavior of the coherence parameters. This behavior can be expressed in physical terms as suggested by McConkey and co-workers.[20] The scattering angles at which the dramatic variation in phase shift or modulation depth occur are those corresponding to particular alignment angles of the excited-state charge cloud.
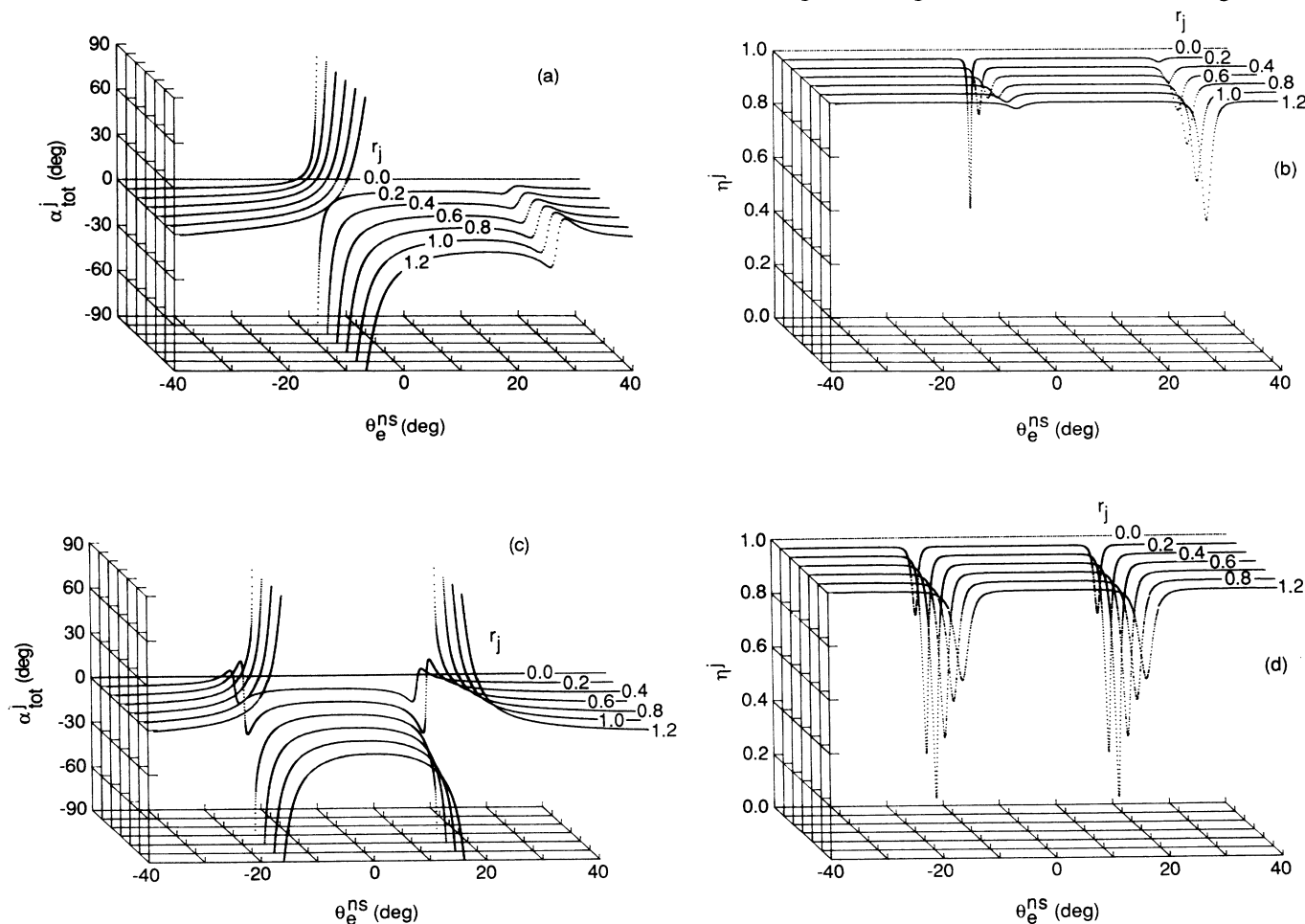

FIG. 4. (a) Modeling results for the variation of total phase shift with θ_e^{ns} for a single scattering point offset from the origin of the laboratory coordinate frame by $\mathbf{r}_j = r_j \hat{\mathbf{Y}}_{ref}$ for r_j values as indicated in mm. The laser beam is in the nominal scattering plane ($\phi_v = 0$) and the λ and χ parameters correspond to $E_0 = 7.24$ eV. The laser polar angles $\theta_v = 45°$. (See text for details). (b) Same as (a) except of modulation depth. (c) Same as (a) except $\theta_v = 90°$. (d) Same as (a) except of modulation depth and $\theta_v = 90°$.

Specifically, when the laser beam views the charge cloud "end on" (i.e., the classical dipole is oscillating along an axis parallel to the laser beam incident vector), the measurement becomes very sensitive to geometrical effects. We have verified that, in all cases, the position of the observed dramatic features corresponds to the case when the laser beam views the charge cloud end on. This is further discussed in Sec. V.

D. Extended scattering volume results

The modeling of superelastic scattering from an extended source requires that we approximate this source by an appropriate collection of scattering points and take a weighted average of the contributions from all points. The intensity for a particular point, specified by a subscript j, is

$$I_j^S(\psi^j) \propto A_j + B_j'\cos2\psi^j + B_j''\sin2\psi^j . \tag{48}$$

The total superelastic signal I_Σ^S arises from the weighted average over all the contributions

$$I_\Sigma^S(\psi_v) = \sum_j a_j I_j^S(\psi^j) , \tag{49}$$

and is given by

$$I_\Sigma^S(\psi_v) \propto A_\Sigma + B_\Sigma'\cos2\psi_v + B_\Sigma''\sin2\psi_v , \tag{50}$$

where

$$A_\Sigma = \sum_j a_j A_j , \tag{51a}$$

$$B_\Sigma' = \sum_j a_j (B_j'\cos2\delta\psi^j + B_j''\sin2\delta\psi^j) , \tag{51b}$$

$$B_\Sigma'' = \sum_j a_j (B_j''\cos2\delta\psi^j - B_j'\sin2\delta\psi^j) . \tag{51c}$$

The form of Eq. (50) allows us to define a modulation depth and phase shift in analogy with the single-point studies,

$$\eta_\Sigma = (B_\Sigma'^2 + B_\Sigma''^2)^{1/2}/A_\Sigma \tag{52}$$

and

$$(\alpha_{tot})_\Sigma = \tfrac{1}{2}\tan^{-1}(-B_\Sigma''/B_\Sigma') . \tag{53}$$

Note that, unlike the single-point-scattering case [Eq. (45)], $(\alpha_{tot})_\Sigma$ is defined by the inverse tangent relation in Eq. (53) since the contributions from the frame-dependent source of the phase shift ($\delta\psi^j$) are accounted for implicitly in B_Σ' and B_Σ''. The a_j factor weights the distribution of scattering points. This weighting would, ideally, reflect the spatial intensity profile of the incident electron beam, the spatial variation in detector response, weighting by the differential (superelastic) cross section over the range of scattering angles defined by the extended source, as well as the spatial distribution of excited state scatterers (which is determined by the target beam distribution, the laser beam intensity profile, and the optical pumping process). Normalization is chosen such that

$$\sum_j a_j = 1 . \tag{54}$$

Our model consists of an incoming parallel electron beam of Gaussian spatial profile which intersects the array of points representing the scattering volume. The incoming laser is also assumed to be parallel but not necessarily lying in the nominal scattering plane (i.e., ϕ_v is kept adjustable). In a real experiment, signal counts are registered for superelastic electrons scattered into the detector view cone. The solid angle of detection is determined by two collimating apertures and the spatial response of the subsequent electron optics (which is difficult to assess). For each scattering point, the collimating apertures define a solid angle, generally different for each point, in which detection of the scattered electrons can occur. Thus, for each scattering point, a range of $\hat{\mathbf{k}}_f$ vectors is possible. Our model takes this into account by performing calculations for a discrete set of $\hat{\mathbf{k}}_f$ limited in direction by the solid angle associated with a particular point in the scattering array. Each term in the sum over j in Eq. (49) thus represents a sum over each $\hat{\mathbf{k}}_f$ allowed by the defined solid angle of detection. It should be emphasized that each different $\hat{\mathbf{k}}_f$ used in the calculation defines a different collision frame as examined above. Therefore, although Eq. (49) explicitly shows only j terms in the summation, there are actually j times i "single point" calculations required if we represent the detector solid angle associated with the jth point by i discrete $\hat{\mathbf{k}}_f$ vectors. The magnitude of this solid angle gives the contribution to a_j of the detector response considering vignetting by the collimating apertures only. The optics themselves, however, introduce a spatial weighting which may considerably "tighten" the spatial detection sensitivity profile expected from the aperture geometry alone. It is argued in Sec. IV that this is indeed an important effect.

For the sake of a reduced computational effort, we have adopted the following simplification in describing the averaging effect of the detector view cone. The system of two collimating apertures is replaced in the model by a single aperture at a distance of $r_{det} = (s + d)$ from the target. The i different $\hat{\mathbf{k}}_f$ vectors are produced by extending rays from an array of i "detection" points lying within this aperture to the jth scattering point (Fig. 5). The unknown detector spatial response is simulated by a two-dimensional Gaussian weighting function of adjustable half-width (centered on the detector axis), which is imposed on the points representing the scattering volume. Our experimental arrangement allows us to neglect the contribution to the spatial distribution of excited-state scatterers from the optical pumping induced by a laser beam of nonuniform intensity profile. This is discussed further in Sec. IV, but the significant point is that the laser spot at the interaction region is many times larger than the scattering volume. Also, to further save computation time, we have represented both the detector and electron beam spatial profile by a single two-dimensional Gaussian centered about the electron beam axis. Such a simplification is justifiable since the product of the Gaussian representing the detector response with the Gaussian representing the electron beam profile gives rise to a new Gaussian of different half-width. This is strictly true at 0° nominal scattering angle only but, for a
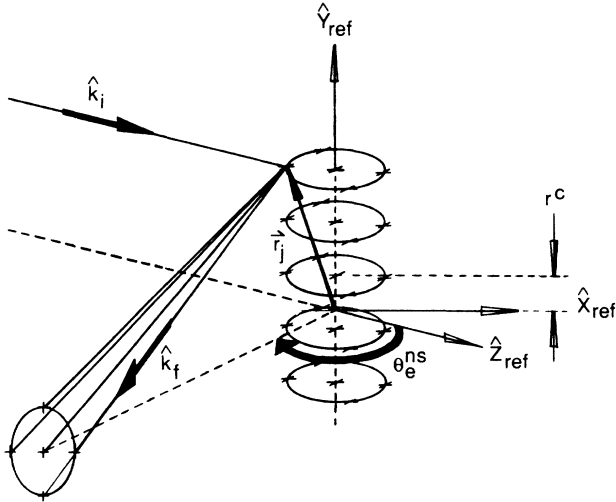
FIG. 5. Schematic diagram for superelastic scattering for a standard extended scattering volume with 25 scattering points.

scattering volume whose width is much smaller than the Gaussian half-width, it is a reasonable approximation even at higher nominal scattering angles. We have also neglected the weighting due to the superelastic DCS.

We have employed several representations of the scattering volume in the modeling. In one case, a three-dimensional volume consisting of five disks equidistantly spaced along $\hat{Y}_{ref}$ with five scattering points per disk, arranged as indicated in Fig. 5, was used, while in the other case a one-dimensional array of five scattering points equidistantly spaced along $\hat{Y}_{ref}$ was used. The three-dimensional volume was constructed to rotate along with the detector as the nominal scattering angle was changed. This was done so that the distribution of scatterers observed by the detector did not change with nominal scattering angle. Modeling results using these different configurations, as well as similar configurations comprising a different overall number of scattering points (for example, three-dimensional volume with 45 points or one-dimensional volume with 11 or 21 points), indicated that the one-dimensional five-point scattering volume results contained the essence of the extended volume effect. For this reason, we carried out most of the extended volume calculations in the five-point one-dimensional approximation to the scattering volume with the five points equally spaced over a 2 mm length. We will refer to this geometry as the standard extended volume. In order to examine the effect of an asymmetrically distributed scattering volume, we moved the symmetric array of scattering points along the $\hat{Y}_{ref}$ axis by some positive or negative offset, r^c with respect to the nominal scattering plane.

Results are presented in Figs. 6(a)–6(d) where we have used coherent parameters (λ and χ) corresponding to 7.24-eV inelastic impact energy. Comparison of these figures with the single point calculations [Figs. 4(a)–4(d)] shows that the behavior of η_Σ with θ_e^{ns} is exaggerated by the averaging, whereas the behavior of $(\alpha_{tot})_\Sigma$ with θ_e^{ns} is moderated somewhat. The exaggeration of the η_Σ behav-

ior can be understood because a contribution to this behavior comes from the single-point η behavior as well as the single-point phase-shift behavior. The sum of $I_j^S(\psi_v)$ modulations with various phase shifts results in a "smearing out" of the modulation curve. The example of a scattering volume comprising two single-point scatterers equally weighted and distributed symmetrically along the $\hat{Y}_{ref}$ axis (with respect to the nominal scattering plane) can illustrate the smearing effect of the summation.

For the upper point

$$I_u^S \propto 1 + \eta^u \cos(2\psi_v + 2\alpha^u + 2\delta\psi^u) \ . \tag{55}$$

For the lower point

$$I_l^S \propto 1 + \eta^l \cos(2\psi_v + 2\alpha^l + 2\delta\psi^l) \ . \tag{56}$$

The single-point calculations show that

$$\eta^u = \eta^l = \eta, \quad \alpha^u = -\alpha^l \ . \tag{57}$$

We also have $\delta\psi^u = -\delta\psi^l$. Thus the weighted sum which gives the overall superelastic signal is

$$I_\Sigma^S \propto 1 + \eta \cos(2\alpha + 2\delta\psi)\cos2\psi_v \ , \tag{58}$$

where the u and l subscripts have been dropped. Two properties of I_Σ^S are evident from Eq. (58). First, the phase shift disappears from the $\cos2\psi_v$ term for symmetrically distributed scatterers and, second, the modulation depth is reduced by the phase-shift-dependent factor $\cos(2\alpha + 2\delta\psi)$. For asymmetrically distributed scatterers, the phase shift no longer cancels completely, leaving a residual phase shift in I_Σ^S. Modeling results obtained with coherence parameters corresponding to 10, 30, and 100 eV impact energies are also shown below.

IV. EXPERIMENTAL RESULTS

The experimental arrangement that we employed was the same as that described by Register et al.[7] We extended their measurements to lower impact energies and to wider angular ranges and devised a way of influencing the scattering geometry in a controllable way.

In order to preserve the optical alignment of electron gun, detector, and target beam, we tuned the gun and detector to pass the incident electron beam to the nose cone of the channeltron when the detector was positioned at zero nominal scattering angle determined by optical alignment. For a series of measurements obtained at various nominal scattering angles but at a fixed impact energy, the source and detector tuning remained unaltered. We checked the zero nominal scattering angle obtained by optical alignment against the forward peaking $Ba(6s^2\,^1S \rightarrow 6s6p\,^1P_1)$ scattering process and applied a correction if a difference was found. An additional He gas target beam was introduced to allow us the calibration of impact energy to the 19.36 eV $He^-(2\,^2S)$ resonance in the elastic channel at 90°. The Ba beam, issuing from a 0.11-cm-diam orifice at the top of a heated tantalum crucible, was collimated by another 0.11-cm-diam aperture yielding an aspect ratio of about 15. Care was taken to ensure that the Ba beam density was kept low

enough not to incur the depolarizing effect of radiation trapping. This condition was checked by monitoring a well-modulated superelastic scattering signal for changes in the degree of modulation while varying the oven temperature.

Our experimental data concerning the overall phase shift and modulation depth are compared to the modeling results in Figs. 7–10 at $E_0^S=5$, 10, 30, and 100 eV for laser configurations $\theta_v=45°$ and 90° ($\phi_v=0°$). The imperfect agreement with the modeling calculations reflects possibly imprecise values of λ and χ parameters and imperfect modeling of the scattering geometry (the results are sensitive to both).

The sign of the total phase shift is determined by the direction of the offset of the extended scattering volume from the symmetric position with respect to the nominal scattering plane. We found that this offset is mainly determined by the tuning and associated sensitivity function of the detector (as discussed in more detail below). It is understandable, therefore, that in some experiments, the phase shift behavior "flipped" with respect to other similar experiments (e.g., in Figs. 9 and 10 the $\theta_v=45°$, $E_0=30$ and 100 eV cases). Note that the modeling calculations presented in Sec. III can account for this effect. The "flipping" of the phase-shift behavior seems to imply that, in some instances, the scattering volume was offset

toward the $+\hat{Y}_{ref}$ axis while, in other cases, a negative offset is indicated. A careful reinvestigation of the results of Register et al.[7] also reveals this flipping in a few cases at 30 and 100 eV. These investigators, however, disregarded the sign of the phase shift and always plotted their results according to a convention which indicated positive phase shift with respect to the zero phase shift they assumed at large negative θ_e^{ns} values. With this clarification, we can also state that the results of Register et al. concerning the phase shift are consistent with the present measurements and modeling calculations. We point out that our phase-shift results (both experimental and modeled) have been plotted modulo π. Comparison with the data presented by Register et al. requires that the difference in presentation between the present paper and that earlier work be kept in mind.

The same general remarks can be made for the comparison of experimental and modeling results concerning the modulation behavior as for the phase-shift behavior. The perfect (i.e., 100%) modulation expected for an LS-coupled target is severely changed by the extended geometry effect over a wide range of angles. The modeling results more closely approach the experimental data in some cases if one allows for ϕ_v to deviate somewhat from the assumed $\phi_v=0$ value. This is demonstrated in Figs. 7(c) and 7(d).
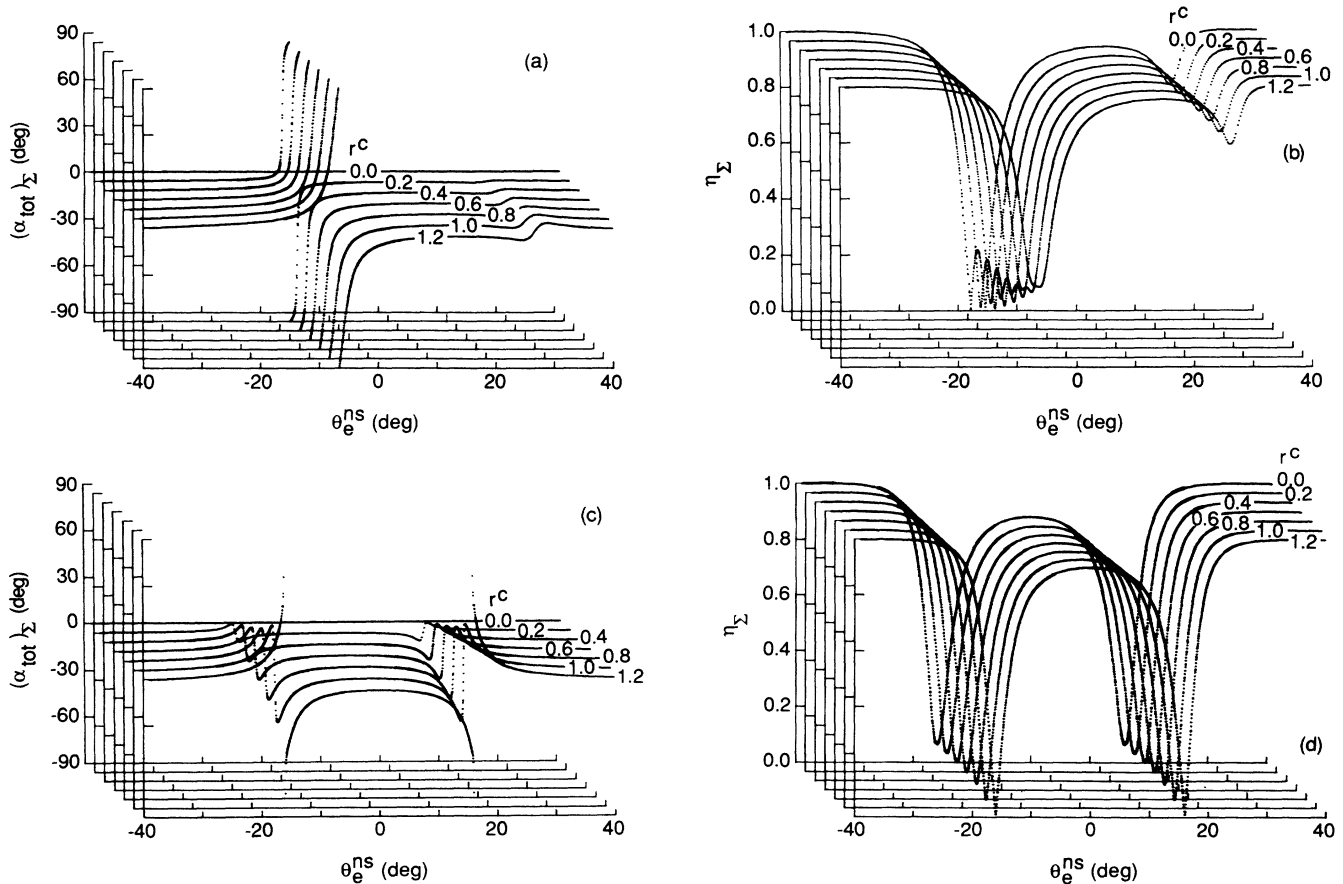

FIG. 6. (a) Modeling results for the variation of total phase shift with θ_e^{ns} for an extended scattering volume as described in the text. The center of the extended volume is offset from the origin of the laboratory frame to r^c as indicated (in mm). The laser beam is in the nominal scattering plane ($\phi_v=0$) and the λ and χ parameters correspond to $E_0=7.24$ eV. The laser polar angle $\theta_v=45°$. (b) Same as (a) except of modulation depth. (c) Same as (a) except $\theta_v=90°$. (d) Same as (a) except of modulation depth and $\theta_v=90°$.

The other aim of the investigation was to devise a means of influencing the geometry in a controllable way. Our modeling results imply that some asymmetry must be present in our effective scattering volume with respect to the nominal scattering plane. We now describe our efforts to understand the nature of this asymmetry and change it in a controlled fashion. Spatial profiles of the laser beam, electron beam, or detector view cone that are asymmetric with respect to the nominal scattering plane could produce an asymmetrically distributed scattering volume as could any misalignment of these beams. Turning our attention to the laser reveals that the laser intensity profile can be symmetric but the nature of the pumping process results in an asymmetric distribution of excited-state atoms. Rate equation calculations by Nickel and Trajmar[21] show that, because of a finite branching ratio for spontaneous radiative decay to the Ba$(6s5d\ ^1D,^3D)$ metastable states, a "leak" exists in the two-level system $(6s^2\ ^1S$ to $6s6p\ ^1P_1)$ coupled by the laser. Although this branching ratio is relatively small ($\sim 350{:}1$),[22] the large number of pumping cycles (~ 100) which an atom undergoes during its travel through the scattering volume causes this leak to be non-negligible and an asymmetry in the excited-state spatial profile results. However, both Register et al.[7] and the present authors have attempted to change the degree of asymmetry of this type by displacing the laser-target intersection spot. No effect on the phase-shift behavior was observed. This implied that the size of the scattering volume was not determined by the laser but by the view cone or electron beam intersection with the target beam. For a view cone or electron beam that samples only a portion of the excited-state target distribution, the asymmetry over this portion is small and the only effect of moving the laser spot is to reduce signal intensity—as observed. We next surmised that intersection of the electron beam with the target beam predominantly above or below the nominal scattering plane was the source of the asymmetry. However, we deflected the electron beam vertically up or down without affecting the phase-shift behavior. This negative result was also found by Register et al.

The above experiments indicated that the extent of the scattering volume may have been limited by an *effective* detector view cone which must have been narrower than that anticipated by considering only the vignetting of the two collimating apertures. The persistence of the phase-shift behavior under a variety of experimental conditions might then be attributed to a bias in the detector optics which favors the detection of electrons that do not travel parallel to the detector axis. Such a directional bias might be introduced by the particular tuning mode in which the detector is set up. Register et al. consistently tuned the detector to maximize the superelastic signal. For the data presented here, we always tuned the detector to pass the incident electron beam at the zero angle established by optical alignment. To confirm these assumptions, we focused the laser beam down to a small size (~ 0.05 cm diam) at the scattering region and thus generated a volume of excited-state scatterers comparable in size to that selected by the detector optics. Furthermore, we introduced a pair of electrostatic deflectors be-

tween the detector collimating apertures in the vertical direction. These modification allowed us to move the distribution of excited-state scatterers up and down by moving the focused laser spot up and down and to subsequently force the detector to look at this displaced distribution by tuning the electrostatic lens train in the detector. With these modifications, we could regain the scattering intensity which was lost by the movement of the laser spot and we were able to cause variation in the phase-shift behavior which was quite large and corresponded to the predicted sign. Only a small fraction of a millimeter movement of the laser spot was required to generate large phase shifts.

V. DISCUSSION AND CONCLUSIONS

We have presented calculations which model the superelastic scattering from an ensemble of ^{138}Ba$(6s6p\ ^1P)$ atoms prepared by "in-plane" linearly polarized laser excitation. The results of these modeling calculations have been expressed in terms of two quantities, the modulation phase shift and the modulation depth, which together completely specify the functional dependence of the superelastic scattering intensity on the laser polarization angle ψ (for a relative intensity measurement). These quantities have been measured experimentally in the present work and comparison with the modeled results shows excellent agreement considering the simplicity of the model adopted. The results of the calculations also explain the puzzling observations made by Register et al.[7]

The modulation phase shift was shown to be due to the fact that the ensemble of scattering points which contribute to the superelastic signal are asymmetrically distributed with respect to the nominal scattering plane. The connection between the phase shift and asymmetry was recognized in the work of Register et al.,[7] but the explanation for this asymmetry was not realized because of two important facts. First, they assumed that the experiments could be interpreted in terms of an ideal, pointlike scattering. Second, with the apparatus and experimental configuration used in their work, it is very difficult to affect the scattering geometry and cause a subsequent change in the phase shift. Their effort was concentrated at 30 and 100 eV impact energies and $\theta_v=45°$ and $\phi_v=0°$ laser geometry. We have found, during the course of the present work, that this experimental configuration is unfavorable for investigating experimentally the dependence of the phase shift on a purposely misaligned scattering geometry. This is due to the fact that [as can be seen from Figs. 9(a) and 10(a)], under these conditions, the phase shift undergoes an excursion through 180° at near-zero nominal scattering angles and the shape of this rapid variation is very similar for different magnitudes of the offset of the scattering volume. The fact that they found this behavior to be reproducible, despite attempts to deliberately change the scattering conditions, is due partly to this particular behavior of the phase shift, partly to the high spatial selectivity of their detector (as explained in Sec. IV), and partly to the procedure adopted by them to optimize the tuning of the instrument on the superelastic

signal. As noted above, in a careful reexamination of the large number of measurements carried out by Register *et al.*, we found a few examples where the sign of the phase shift was reversed (they did not consider the sign of the phase shift in their analysis). Apparently, the tuning of the detector in these few cases was such that the center of gravity of the scattering volume fell on the opposite side of the nominal scattering plane. It took us a special effort and modification of the apparatus and tuning procedures to be able to clearly demonstrate the connection between the modulation phase shift and the scattering geometry. The modeling calculations indicated that the best conditions for carrying out these experimental checks corresponded to $\theta_v = 90°$ and a 5-eV impact energy. With these conditions, we were able to introduce large phase shifts by slight movement of the focused laser spot. In principle, it is possible to produce a scattering arrangement which eliminates the phase shift, but we have not been able to establish such conditions in the several attempts that we made (although some of our data indicate that we were close). Further confirmation of the geometrical cause of the phase shift comes from the ability of our model calculations to reproduce the experimentally observed phase shift at impact energies ranging from 5 to 100 eV. Considering the somewhat crude modeling of the extended scattering volume and the uncertainties associated with the calculated λ and χ

parameters, the agreement is excellent. As far as the phase shift is concerned, we conclude that, in principle, it could be fully eliminated, but in practice this may not be easy to achieve.

The second aspect of our findings (which is even more important than the modulation phase-shift behavior) is the behavior of the modulation depth of the superelastic scattering signal. In general, the coherence parameters are extracted from the scattering-angle dependence of this modulation depth. The deviation of this modulation depth from one (which is the value expected at all scattering angles in the ideal single-point scattering picture for an *LS*-coupled target and $\phi_v = 0°$) can be interpreted as signifying the importance of spin-orbit-coupling effects. In our modeling calculation, we assumed that the *LS*-coupling scheme was valid and demonstrated how geometrical effects alone cause the modulation to deviate from the value of unity. (This deviation persists both for symmetric and asymmetric distributions of scattering points.)

If spin-orbit coupling were present, then the deviation of modulation from unity would be partly due to spin-orbit coupling and partly to geometry. It is clear from Figs. 7–10 that the geometrical effects on the modulation are large over appreciable ranges of nominal scattering angles. In some cases, the modulation completely disappears at nominal scattering angles far from zero. The an-
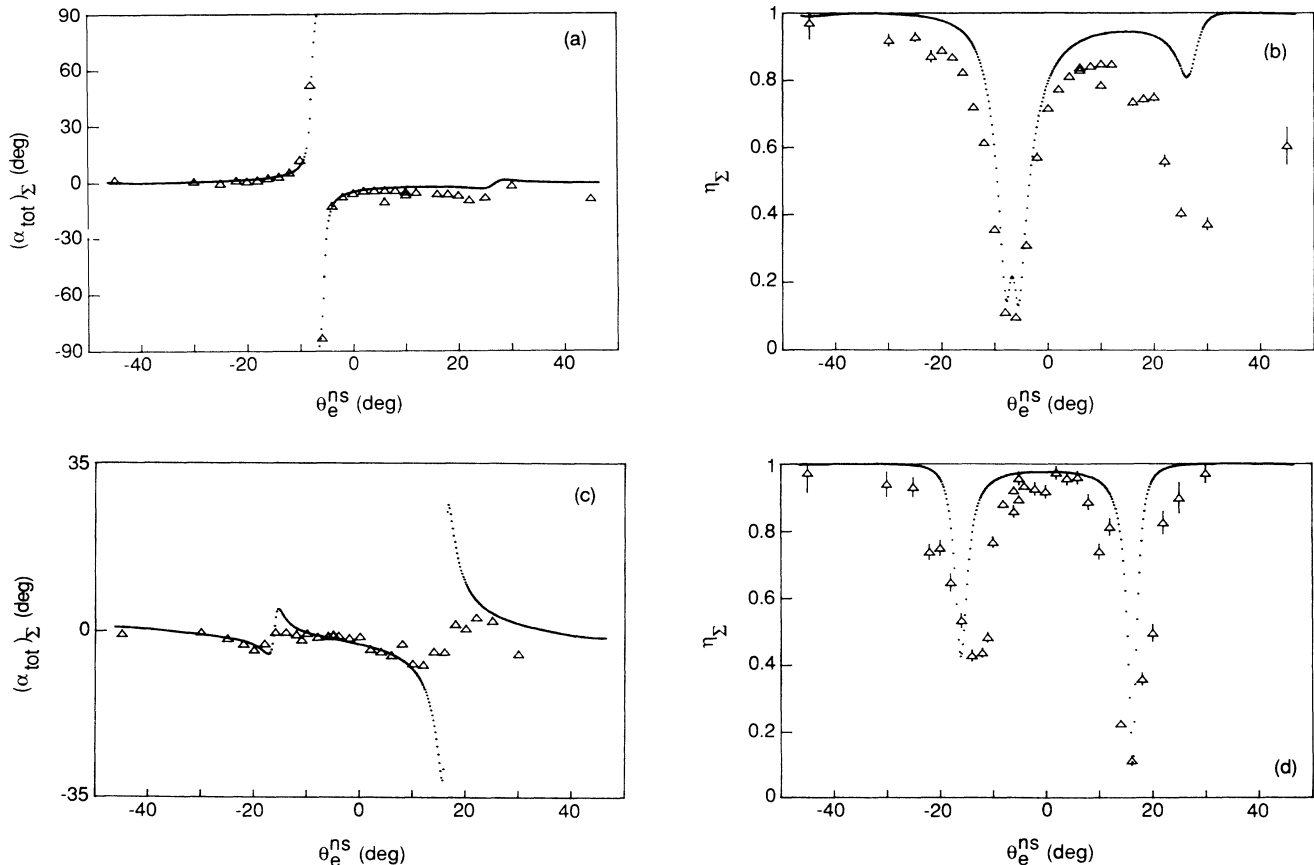

FIG. 7. (a) The variation of total phase shift with θ_e^{ns} at $E_0^s = 5.0$ eV, $\theta_v = 45°$, and $\phi_v = 0°$. Experimental results are indicated by triangles and the modeling results by dotted lines. In the model a standard extended volume located at $r^c = 0.2$ mm was used. See text for more explanation. (b) Same as (a) except for modulation depth. (c) Same as (a) except for $\theta_v = 90°$, $\phi_v = 2°$. (d) Same as (a) except for modulation depth and $\theta_v = 90°$, $\phi_v = 2°$.
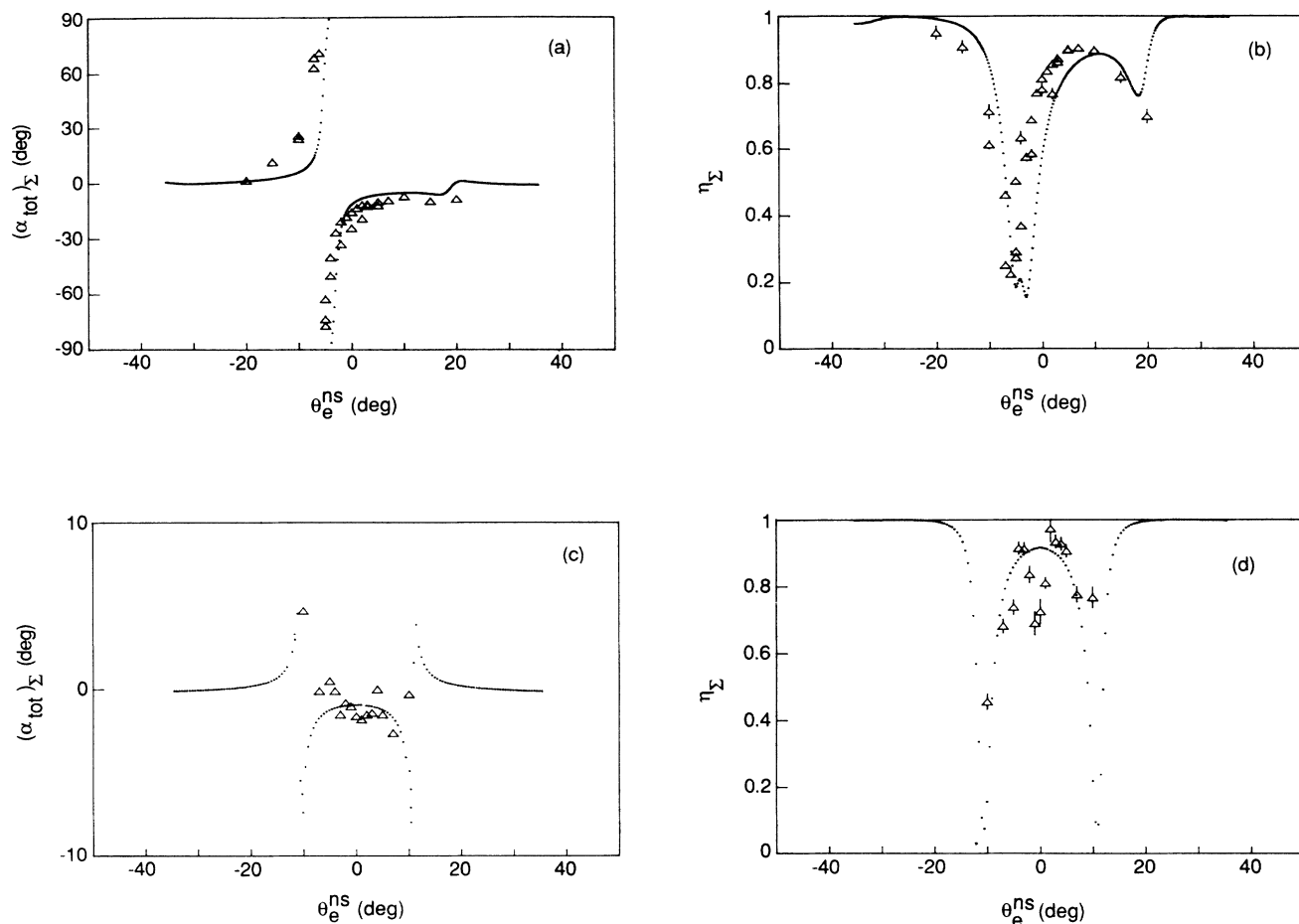
FIG. 8. (a) Same as Fig. 7(a) except $E_0^s=10.0$ eV. (b) Same as (a) except for modulation depth. (c) Same as (a) except for $\theta_v=90°$. (d) Same as (a) except for modulation depth and $\theta_v=0°$.

gular range of these large deviations strongly depends on the behavior of the coherence parameters. We have found that the location of the dramatic dips in modulation depth (and the corresponding rapid excursions undergone by the modulation phase shift) occur when the "major axis" of the excited-state charge cloud (assuming an approximately p-type orbital) is parallel to the laser beam incidence vector. In other words these effects appear when the laser beam incidence vector coincides with the minimum in the angular intensity distribution of radiation (polarization averaged) emitted by the excited atom. The angular intensity distribution of emitted radiation is given by the coefficient A [in Eq. (21)] so that a minimum in this distribution occurs when A is a minimum. We have found that A is relatively insensitive to offset scattering while B', and particularly B'', are affected to a much greater extent. Hence the ratio which defines η [Eq. (42)] becomes very sensitive to changes in B' and B'' near the minimum in A. Therefore a complex interplay

between scattering geometry and coherence parameters is responsible for the observed effects on the modulation depth and phase shift. We stress again, however that all of the modulation effects observed for superelastic scattering on $^{138}Ba(6s6p\ ^1P_1)$ are manifestations of a finite scattering volume, possibly but not necessarily, asymmetrically situated with respect to the nominal scattering plane. For a single-point scattering event occurring at the reference frame origin, the behavior of the modulation depth and phase shift is as expected (i.e., $\eta=1$ and $\alpha=0°$) for our LS-coupled target, regardless of the alignment of the charge cloud with respect to the laser beam incident vector. In principle, one could account for the geometrical effects and thereby deconvolute the coherence parameters. In practice, however, this would be very difficult (if not impossible) since the scattering geometry is not known well enough.

An interesting demonstration of the influence of the scattering geometry can be made by calculating the
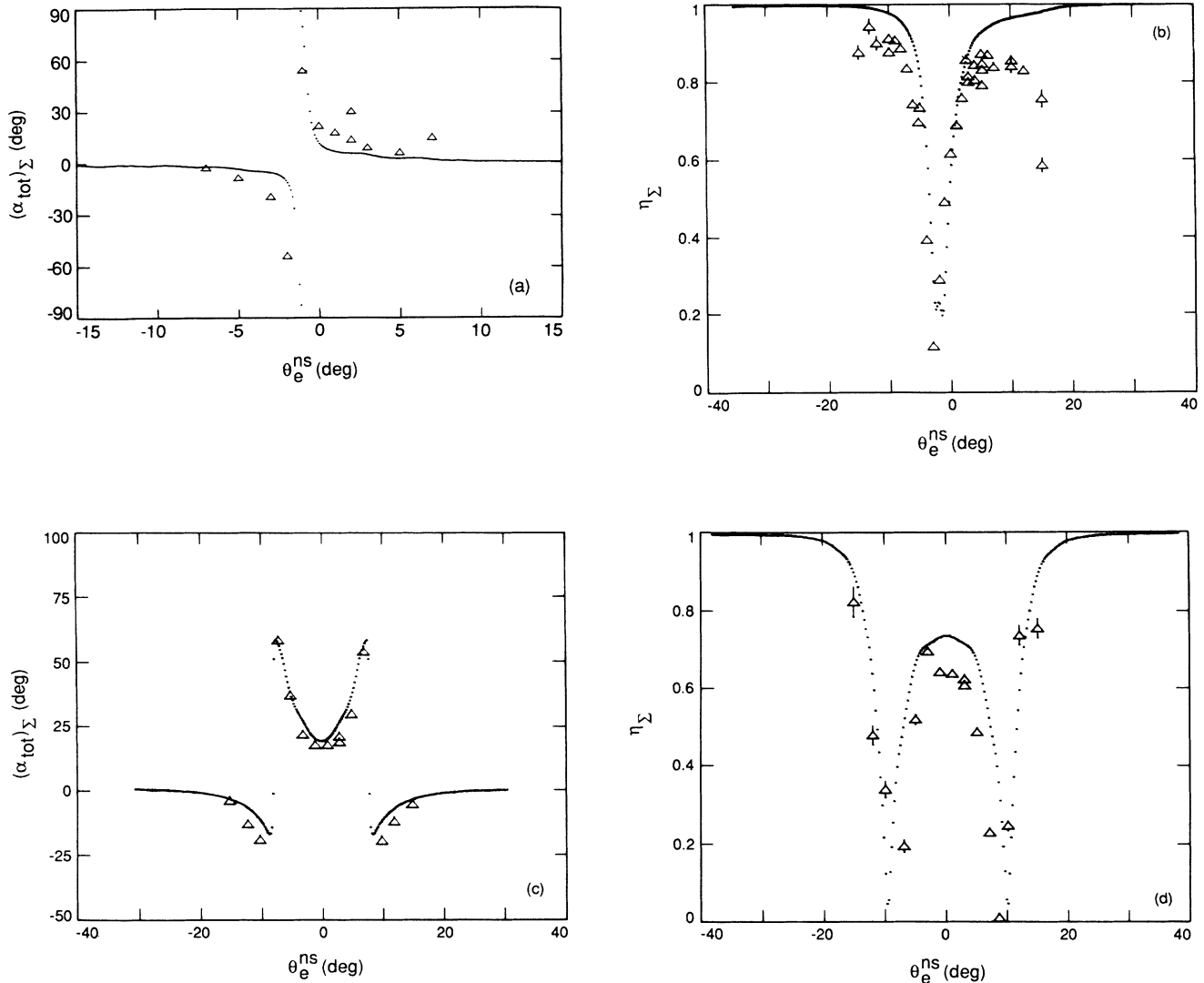
FIG. 9. (a) Same as Fig. 7(a) except $E_0^s = 30.0$ eV. (b) Same as (a) except for modulation depth. (c) Same as (a) except for $\theta_v = 90°$. (d) Same as (a) except for modulation depth and $\theta_v = 90°$.

modulation depth for an extended scattering volume as a function of nominal scattering angle for a given set of coherence parameters and then treating the result as experimental data. A set of "apparent coherence parameters" can then be extracted assuming point like scattering. Figures 6(b) and 6(d) show the modulation curves calculated for a superelastic scattering experiment carried out at 5-eV impact energy and laser angles $\phi_v = 0°$ and $\theta_v = 45°$ and 90°. We took as our fictitious experimental data the $r^c = 0$ curves (i.e., a symmetrically located scattering volume). A comparison between coherence parameters extracted from these curves under the assumption of an ideal single-point scattering geometry and the coherence parameters used as input to the modeling code is presented in Fig. 11. It is clear that significant discrepancies exist. However, these discrepancies seem

to be most severe near zero scattering angle, as intuition would suggest. Surprisingly, the agreement between the "apparent" and true coherence parameters is fairly good in the scattering-angle region where extreme distortion of the modulation depth is present. For the results plotted in Fig. 11, finite scattering volume effects cause the modulation depth to decrease to near zero at $\theta_e^{ns} = -5.5°$ ($\theta_v = 45°$) and at $\theta_e^{ns} = \pm 15.5°$ ($\theta_v = 90°$). At $\theta_e = 5.5°$, the extracted apparent coherence parameters deviate quite strongly from the true coherence parameters, but at $\theta_e = 15.5°$ the discrepancy is relatively small. The explanation of this arises from the fact that, in order to extract three coherence parameters, three values of the modulation depth $\eta(\theta_v, \theta_e^{ns})$ are required: $\eta(45°, +\theta_e)$, $\eta(45°, -\theta_e)$, and $\eta(90°, +\theta_e)$ or $\eta(90°, -\theta_e)$. The distorted behavior in one particular $\eta(\theta_v, \theta_e^{ns})$ over a particu-
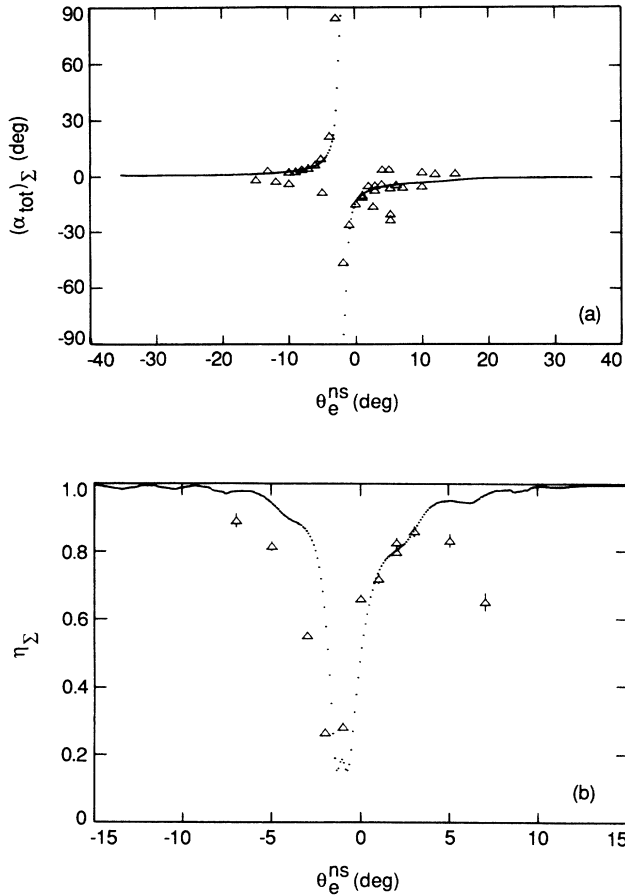
FIG. 10. (a) Same as Fig. 7(a) except $E_0 = 100.0$ eV. (b) Same as (a) except for modulation depth.

lar range of θ_e^{ns} is, in the situations we have encountered, accompanied by reasonably undistorted behavior in the other two η measurements over the same region of θ_e^{ns}. Thus in some cases (i.e., the $\theta_e = 15.5°$ measurement presently under discussion) the largest contribution to the extraction of an apparent coherence parameter is made by the "well-behaved" modulation depths. We caution that it is impossible to predict a priori whether such a fortunate circumstance will prevail over a specified range of θ_e^{ns}. Although in the present case, reasonable coherence parameters can be extracted over a range of scattering angles where η behaves "badly," there is no reason to expect this to be generally true.

In summary, we can state that modeling calculations and supporting experiments show that the interpretation of superelastic scattering measurements for "laser inplane" geometry can be highly uncertain due to geometrical effects. Nominal scattering angles at which dramatic effects are observed are determined by the particular experimental configuration and the behavior of the coherence parameters. Extraction of coherence parameters from experimental data under the assumption of an ideal scattering geometry (pointlike scattering source located at the origin of the laboratory, reference coordinate

frame) can lead to serious errors in these parameters and consequent incorrect conclusions about spin-orbit-coupling effects. A report[23] with the same title and authors is an extended version of this article and contains the details of theoretical derivations.
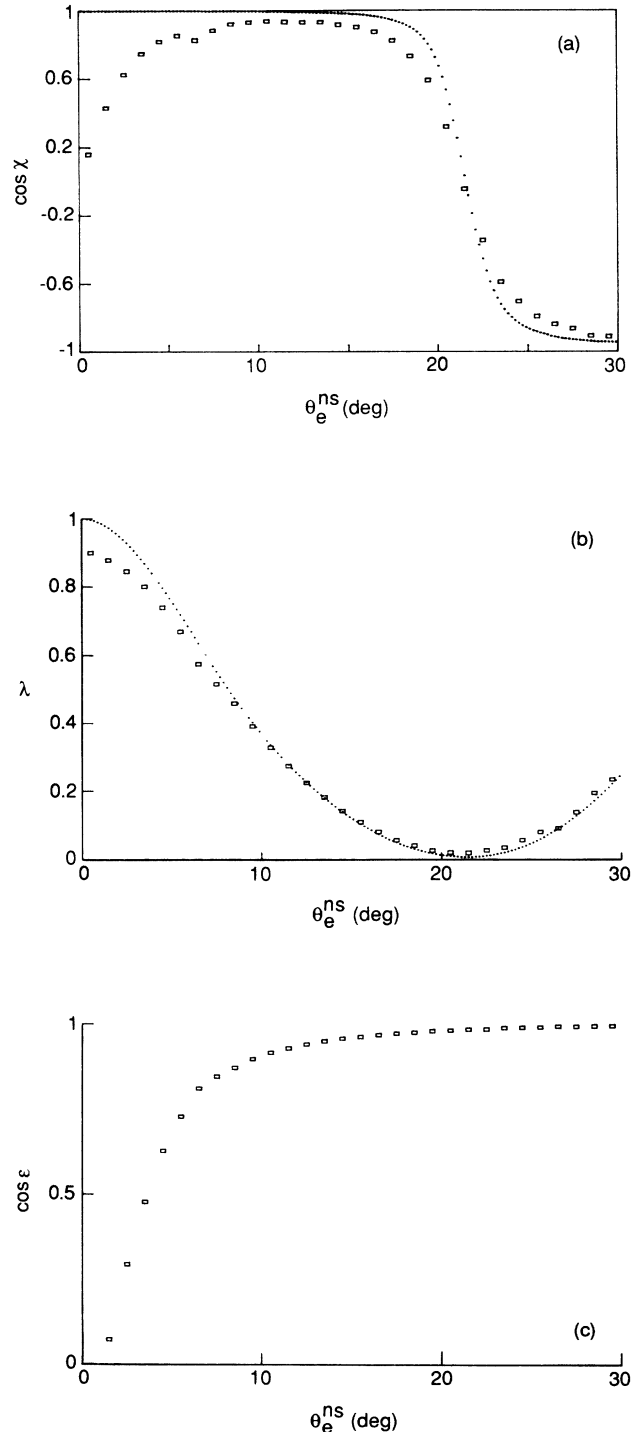

FIG. 11. (a) The actual and "apparent" values of $\cos\chi$. See text for explanation. (b) Same as (a) except for λ. (c) Same as (a) except for $\cos\epsilon$.

ACKNOWLEDGMENTS

*Permanent address: Department of Physics, University of Manitoba, Winnipeg, Manitoba, Canada R3T 2N2.

[1] R. T. Brinkmann and S. Trajmar, J. Phys. E **14**, 245 (1981).

[2] M. Eminyan, K. B. McAdam, J. Slevin, and H. Keinpoppen, Phys. Rev. Lett. **31**, 576 (1973); J. Phys. B **7**, 1519 (1975).

[3] K. Blum and H. Kleinpoppen, Phys. Rep. **52**, 203 (1979); Adv. At. Mol. Phys. **19**, 187 (1983).

[4] I. V. Hertel and W. Stoll, J. Phys. B **7**, 570 (1974); **7**, 583 (1974); Adv. At. Mol. Phys. **13**, 113 (1977).

[5] N. Andersen, J. W. Gallagher, and I. V. Hertel, Phys. Rep. **165**, 1 (1988).

[6] K. E. Martus, K. Becker, and D. H. Madison, Phys. Rev. A **38**, 4876 (1988).

[7] D. F. Register, S. Trajmar, G. Csanak, S. W. Jensen, M. A. Fineman, and R. T. Poe, Phys. Rev. A **28**, 151 (1983).

[8] R. E. H. Clark, J. Abdallah, Jr., G. Csanak, and S. P. Kramer, Phys. Rev. A **40**, 2935 (1989); R. E. H. Clark and J. Abdallah, invited talk, in *Proceedings of the Fifth International Symposium on Polarization and Correlation in Electronic and Atomic Collisions, Hoboken, NJ, 1989* (U.S. GPO, Washington, DC, in press); R. E. H. Clark (private communication).

[9] P. W. Zetner, S. Trajmar, G. Csanak, and R. E. H. Clark, Phys. Rev. A **39**, 6022 (1989).

[10] J. Macek and I. V. Hertel, J. Phys. B **7**, 2173 (1974); see also I. V. Hertel and W. Stoll, Adv. At. Mol. Phys. **13**, 113 (1977).

[11] U. Fano, Phys. Rev. **90**, 577 (1953).

[12] For reviews on denisty matrices as applied to angular correlation problems, see U. Fano, Rev. Mod. Phys. **45**, 553 (1973); K. Blum, in *Progress in Atomic Spectroscopy*, edited by W. Hanle and K. Kleinpoppen (Plenum, New York, 1978); K. Blum, *Density Matrix Theory and Applications* (Plenum, New York, 1981).

[13] U. Fano and H. J. Macek, Rev. Mod. Phys. **45**, 553 (1973).

[14] F. J. da Paixão, N. T. Padial, Gy. Csanak, and K. Blum, Phys. Rev. Lett. **45**, 1164 (1980); K. Blum, F. J. da Paixão, and Gy. Csanak, J. Phys. B **13**, L257 (1980).

[15] I. C. Percival and M. S. Seaton, Philos. Trans. R. Soc. (London) Ser. A **251**, 113 (1958).

[16] We adopt here the definition of level and sublevel used by E. U. Condon and G. H. Shortley [*The Theory of Atomic Spectra* (Cambridge University Press, New York, 1935)]. Any energy level corresponding to a given value of J (total electronic angular momentum) is $(2J+1)$-fold degenerate. Such a set of $2J+1$ states or sublevels we shall call a level.

[17] We should also note here that if spin-orbit-coupling effects play a role for the continuum electron then even for unpolarized incident electrons the superelastically scattered electrons may become transversely polarized. For the hypothetical inverse collision process this would mean that the incident electrons are transversely polarized and the inelastically scattered electrons are unpolarized. [See, e.g., J. Kessler, *Polarized Electrons* (Springer-Verlag, Berlin, 1976).]

[18] The Euler angles are defined here as by A. R. Edmonds, *Angular Momentum in Quantum Mechanics* (Princeton University Press, Princeton, 1957), pp. 6–8.

[19] Spin-orbit coupling in the target atom is accounted for by application of the $|nJM_J\rangle$ representation. Spin-orbit coupling for the continuum electron should also be considered. It has been shown, however, that such considerations lead to a formalism which is identical with the treatment of it in the target atom. (See Ref. 3.) The experiments interpreted with the present formalism will therefore yield information on spin-orbit-coupling effects ($\cos\epsilon$ and $\cos\Delta$) which represent these two contributions.

[20] J. W. McConkey (private communication); P. Plessis, M. A. Khakoo, P. Hammond, and J. W. McConkey, J. Phys. B **21**, L483 (1988).

[21] J. C. Nickel and S. Trajmar (unpublished).

[22] S. Trajmar, J. C. Nickel, and T. Antoni, Phys. Rev. A **34**, 5154 (1986).

[23] P. W. Zetner, S. Trajmar, and G. Csanak, Jet Propulsion Laboratory, California Institute of Technology Report No. D-7095, 1990 (unpublished).